

U.S. Department of Commerce
National Institute of Standards and Technology
Materials Science and Engineering Laboratory
Polymers Division
Gaithersburg, MD 20899

RECEIVED
11/10/05

2005 AUG -9 12 3:44

REPORT OF ANALYSIS

March 1, 2005

EA05-005

- Submitted to:** Mr. Bruce York, Department of Transportation, National Highway Traffic Safety Administration, Office of Defects Investigation, 400 7th Street, SW, Washington, DC 20590
- Through:** Eric J. Amis, Chief
Polymers Division
- Authors:** Gale A. Holmes, Da-Wei Liu, Walter G. McDonough, Joy Dunkers, Jean Stephens, Chad R. Snyder
- Title:** Investigation of Ford Speed Control Deactivation Switches – Polymers Division Contributions
- Constituents:** X-ray Photographs, Conductivity Measurements, Dimensional Analysis and Materials Analysis
- Copies to:** No copies retained at NIST. As a record of this document, a copy of this page will be filed by in office of the Polymers Division.

Background: This report is submitted pursuant to the requirements of a contract between NIST and the National Highway Traffic Safety Administration (NHTSA) covering NIST testing of speed control deactivation switches (SCDSs) from Ford vehicles. The NIST Polymers Division was contracted to perform a variety of tests and to provide consultation as directed by the NHTSA Office of Defects Investigation. Figure 1 is a schematic drawing of an SCDS, from a Texas Instruments document provided by NHTSA. This report contains descriptions of work performed and test results obtained by the Polymers Division during the period from about July 1, 2005, until about December 30, 2005, in fulfillment of the contract with NHTSA.

I. Problem Statement

Statistical data have shown that a speed control deactivation switch (SCDS) used in Ford automobiles until 2003 (see Figure 1a) fail at a higher rate in some models. Based on failure rate data collected by NHTSA, NIST was given SCDSs from several product lines (see Table 1) to ascertain what differences in the mechanical properties of the active parts and/or SCDS construction may be contributing to the observed higher failure rates.

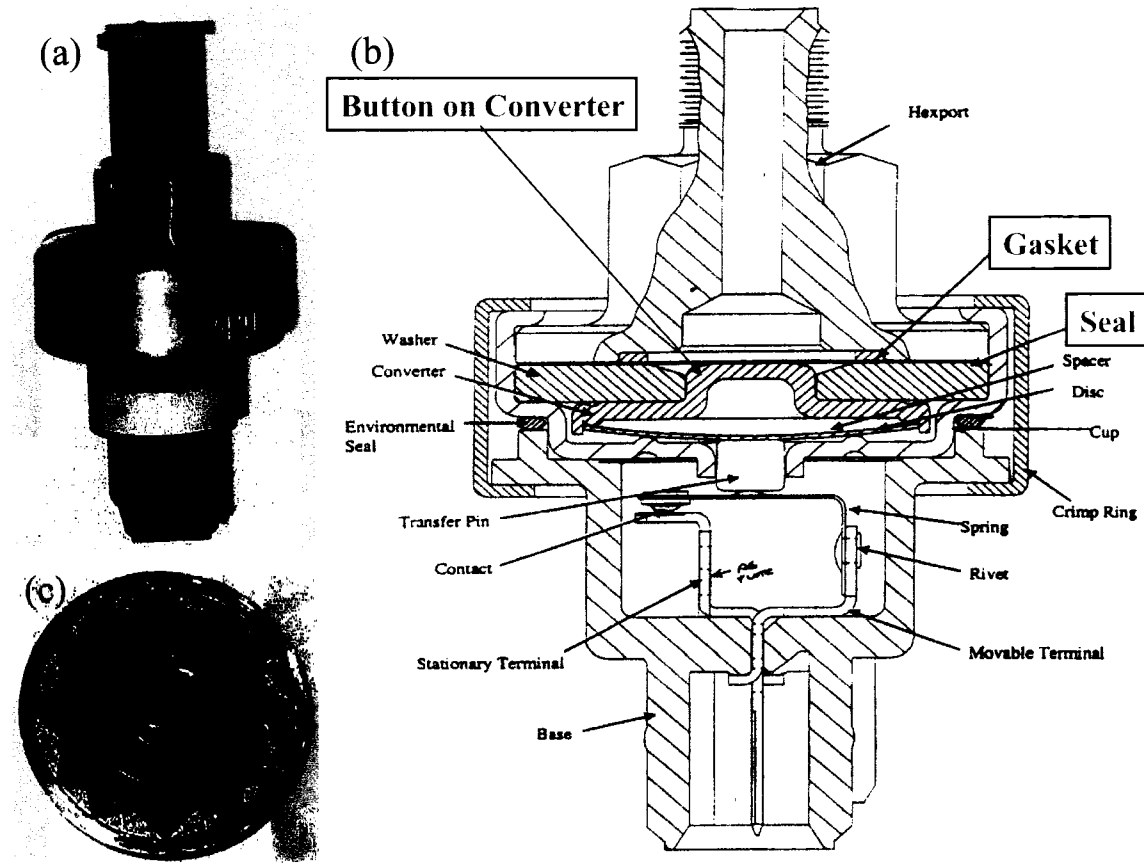


Figure 1. Speed Control Deactivation Switch (SCDS) (a) Assembled (b) Assembly Cross-Section Drawing And Component Labels, and (c) Kapton Seal arrangement.

The bad SCDSs in Table 1 are labeled as Bad No Brake Fluid Remaining (BNBR), Bad With Brake fluid Remaining (BWBR), Light Burn With Brake fluid Remaining (LBWBR), and Leakers. Based on statistical failure rate data, SCDSs that had not failed were labeled Likely Good and Likely (to go) Bad.

Table 1. Grouping of SCDS Supplied to NIST

Bad				Likely Good	Likely Bad
BNBR	BWBR	LBWBF	Leaker		
71	51	4	3	7	32
77	58	9	17	1	6
78	60	45	49	5	30
79	65	46	50	10	35
	67	48	52	14	61
	68	53	55	15	62
	70	59	56	16	82
	72	69	57	18	83
	75	76		19	84
		80		20	85
				26	86
				27	87
				28	88
				29	89
				34	90
				36	91
				38	92
				40	93
					94
					95
					96

II. Background Information

SCDS failure has been linked to the failure of the Kapton[#] seal (labeled Seals in Figure 1b). As shown in Figure 1c, this seal is composed of three layers of 19.05 mm (0.75 in) square Kapton laminate film that is 5 mil (0.125 mm) thick. The Kapton film (DuPont Kapton 500FN131L) is a composite construction consisting of a polyimide film 3 mil (0.075 mm) thickness sandwiched between 1 mil (0.025 mm) thick films of fluorinated ethylene propylene copolymer (FEP). The seal is held in place by a rubber gasket (see Figure 1b).

Polyimides are formed by the polycondensation reaction between an aromatic dianhydride and an aromatic diamine (see Figure 2). The specific polyimide used in the Type FN Kapton film is formed from the reaction of pyromellitic dianhydride and 4,4'-diaminodiphenyl ether. The FEP layers protect the polyimide film from hydrolysis.

[#] Certain equipment, instruments or materials are identified in this paper in order to adequately specify the experimental details. Such identification does not imply recommendation by the National Institute of Standards and Technology nor does it imply the materials are necessarily the best available for the purpose.

Research has shown that even though the structure of FEP resembles that of polytetrafluoroethylene (PTFE), the presence of the bulky perfluoromethyl side group tends to distort the highly crystalline structure of the PTFE chain and results in a higher amorphous fraction. Since organic solvents permeate through the amorphous phase (The crystallite regions are not permeable), it would be expected that FEP is more susceptible to permeation than PTFE. However, since FEP resins are melt processable they are void free and permeation can only proceed via molecular diffusion, unlike in PTFE where both molecular diffusion and porous transport are active. Overall, the permeation characteristics of FEP are slightly superior to those of PTFE.

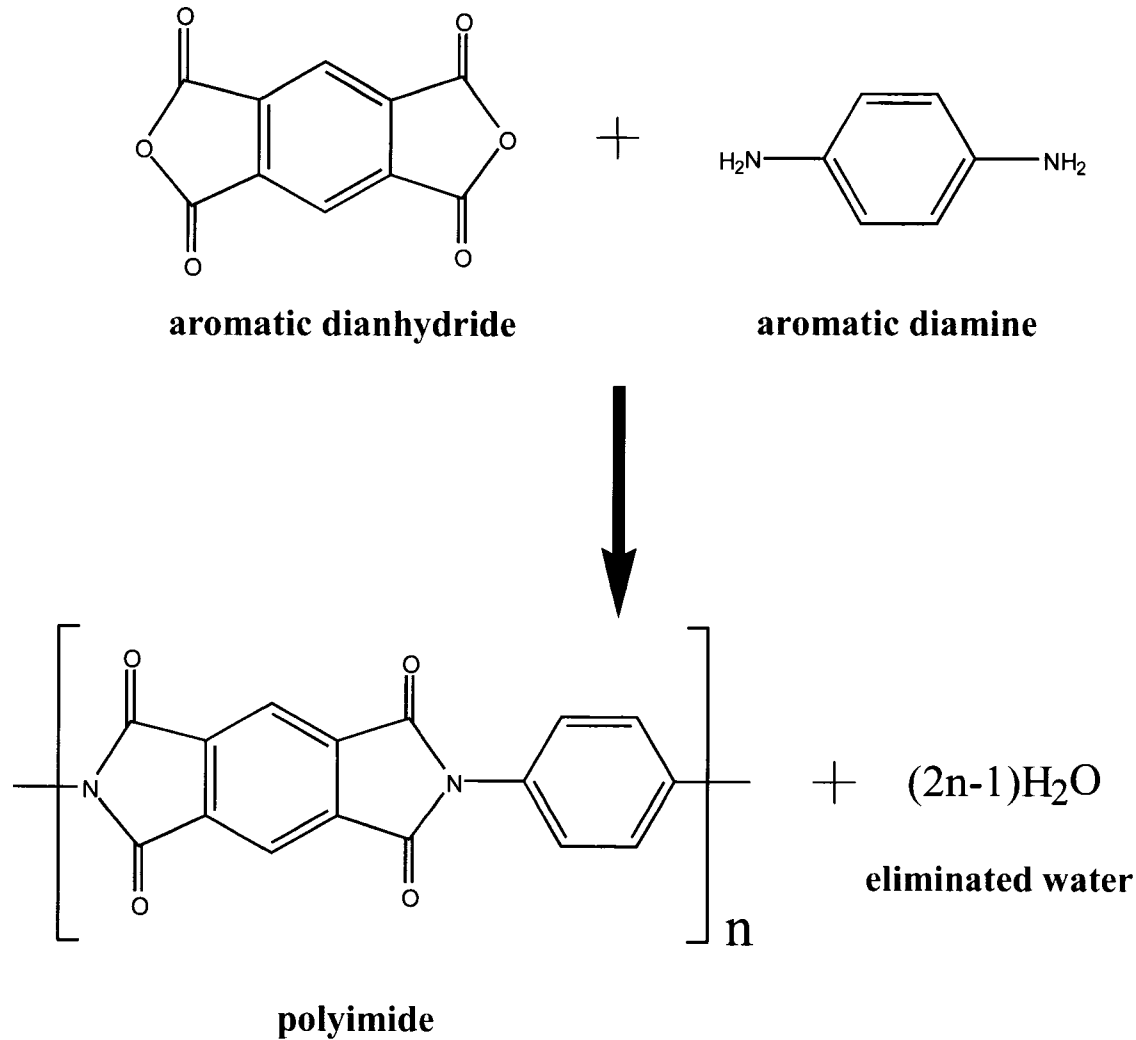


Figure 2. Polyimide polycondensation reaction.

Therefore, failure of the FEP layer can lead to degradation of the polyimide film¹ if moisture is present in the brake fluid. Furthermore, FEP has been shown to have a flex life of only 80,000 cycles before failure, whereas, PTFE can withstand more than 1 million cycles.² Thus, the key

question that needs to be answered is what factors contribute to the accelerated failure of this film in certain Ford automobiles.

Two possible scenarios were put forth by NHTSA. The first suggests that there may be a difference in the mechanical properties of the Kapton seals between the good and bad samples. It is also possible that the properties of the rubber gasket may be different in the good and bad samples.

III. Experimental Procedures

Disassembly and sample collection procedures are described in detail in the Analytical Chemistry Division's report of analysis. Photographs at each stage of the procedure have been provided to NHTSA as electronic files. All measurements of the Kapton film in Sections III.H through III.K, excluding the IR measurements, were performed on samples taken from outside the o-ring crimp region to eliminate effects caused by mechanical fatigue. The three Kapton seals were numbered 1 through 3. Layer 1 faces the brake fluid and Layer 3 faces the converter.

A. Resistance Measurements. Four-wire resistance measurements were performed using a Keithley Model 2000 Digital Multimeter calibrated traceable to NIST on June 14, 2004 by Keithley on a series of Leeds & Northrup Standard Resistors with values of 1 Ω , 10 Ω , 1000 Ω , 10,000 Ω , and 100,000 Ω . Prior to initial measurements, the digital multimeter was zeroed with all four probes shorted together. Measurements on the standard resistors were then made on a Keithley Model 6514 System Electrometer in a two-wire configuration. Absolute error was less than 1 % for the standards at 10 Ω and higher and the difference at 1 Ω was within the resolution of the instruments. Ambient conditions were nominally 55 % relative humidity and 23 $^{\circ}\text{C}$. Measurements were made from Terminal 1 (T1) to Terminal 2 (T2), from T1 to ground (the hexport body), and T2 to ground. See Figure 3 for a schematic of the terminal layout.

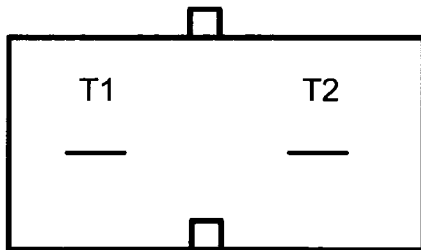


Figure 3. Schematic of terminals at bottom of switch. Note T1 is the terminal from the fuse and T2 is the terminal from the servo.

B. X-ray Photography. X-ray photographs were obtained on each SCDS to determine the state of the terminals in the switch prior to disassembly. Two photographs were taken on each switch at 0 $^{\circ}$ and 90 $^{\circ}$ angles, by the NIST Radiation Physics facility.

C. Optical Images of Kapton Seals. To characterize initial conditions of Kapton seals, optical images were obtained on a Leica microscope equipped with a 1.6x lens. Digital images were taken from the microscope using an Evolution MP color digital camera that was connected to version 5.0 of Q Capture Pro.

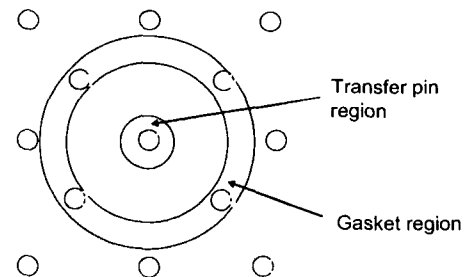
D. Polarized Optical Microscopy. To identify regions of orientation or stress in the seals, bright field and polarized images were obtained using a Leica MZ16 optical stereomicroscope system with high depth of field, adjustable oblique light sources and traveling stage accurate to the nearest micrometer. Magnifications used were 1.6X, 2.5X, 5X, 10X. Regions of interest were interrogated with the higher magnifications.

E. Measurescope Imaging. Using a MM-40 Nikon measuring microscope equipped with a 1x magnifying lens, each Kapton seal layer was observed in the reflection mode.

F. Electron Microscopy. The samples were imaged using a Hitachi S-4700-II field emission-scanning electron microscope (FE-SEM) equipped with an x-ray microanalysis capability for elemental analysis. The samples were gold (Au) coated prior to imaging to reduce charging. Using the FE-SEM, cracked or compromised region of the sample was identified and imaged. The exterior and interior of the crack were analyzed for differences in chemical components.

G. Dimensional Analyses.

(1) *Thickness Measurements* were made on the seals in a ball-to-plane configuration using a caliper fitted with a linear voltage displacement transducer calibrated to 0.1 μm . To assess possible distortions due to the crimping process, 14 measurements were made as per the diagram to the right. All but measurement spot #6 were performed with the ball on the brake fluid side, spot #6 was performed with the plane on the brake fluid side. 45 seals were measured in all 14 spots; the remaining seals were measured only at spots #1, #3, #8, and #10.



(2) *Laminate Layer Thickness Verification.* Because NHTSA raised the possibility that the thickness of the FEP and Kapton layers comprising the laminate were not meeting specifications, cross sectional images were taken of an as-received sample of the Kapton FN500131L laminate, a randomly chosen Likely Good seal, and a randomly chosen LBWBF seal. The samples were embedded in Buehler Ultra-Mount powder (#20-3572) using a 2.54 cm LECO ring mold and a spring clip to hold the sample edge up. After 30 min curing, according to manufacturer's directions, the samples were polished with increasing fine grits of silicon carbide Struers paper, 1200, 2400, and then 4000 grit. The surface was then polished with Buehler diamond of increasingly finer size: 6 μm , 3 μm , and then 1 μm , using Struers DP Lubricant. The samples were then imaged with a Nikon Stage Micrometer at 400x magnification.

(3) *Switch Dimensions.* All thickness measurements were made using a Mitutoyo Digimatic Caliper (Model CD-6"CS). The resolution of the measuring device was

0.01 mm, with an accuracy of ± 0.02 mm and a repeatability of 0.01 mm as specified by the manufacturer.

The thicknesses of four parts of the SCDS were measured: (a) the washer, (b) the o-ring, (c) gasket seat depth, and (d) outside ring thickness (see Figure 4). Each part was measured three times at approximately 120° increments.

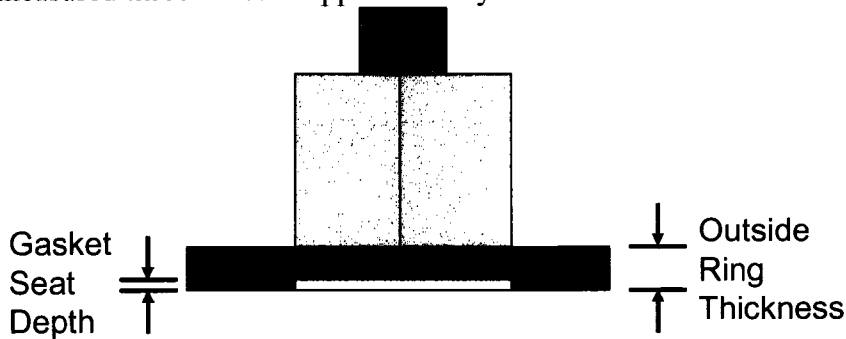


Figure 4. Hexport body measurement schematic.

H. Density. All measurements were made using a Sartorius BP 210 D (Sartorius AG, Goettingen, Germany) electronic balance with a Sartorius Density Determination kit. The procedure that follows is that described in the Density Determination Kit's manual. The method described in the manual applies the Archimedean principle for determining the specific gravity of a solid.

Three sets of measurements were made with different depths of immersion. The first two measurements were made at an immersion depth of approximately 10 mm and the third was made at a depth of 30 mm below the surface of the distilled water. A large diameter (76 mm) beaker was centered on the metal platform on the scale. The beaker was then filled with distilled water to certain levels below the rim of the beaker. Three drops of a surfactant (Tween) were added to the distilled water. A thermometer was attached to the rim of the beaker using a retainer clip. The water was allowed to equilibrate overnight.

The balance was tared, the sample was placed on the upper pan in air and the mass M_a in grams was measured. The balance was then tared again, this time with the sample on the upper pan on the frame. The sample was then submerged and placed on the retaining pan using tweezers. The absolute readout of the buoyancy (G) in grams was then measured. The temperature of the liquid was measured and using the table provided in the manual, the appropriate value of the density (ρ_{fl}) was determined. The density of the material was then calculated using the following formula:

$$\rho = M_a * [\rho_{fl} - 0.0012 \text{ g/cm}^3] / (0.99983 * G) + 0.0012 \text{ g/cm}^3$$

Measurements were only performed on the layer 2 seal, to minimize contamination effects from the brake fluid or converter button.

I. Infrared Analysis of Material. The film sandwiches from layer 2 were analyzed using Fourier transform infrared microscopy (Nicolet Magna 550 spectrometer, Nic-Plan microscope) for chemical information relating to film defects. Reflection spectra were taken using a 32X objective and 64 scans. (Button-up refers to deformation of the Kapton seal caused by the converter button. Button-up is the side facing the brake fluid. See Figure 1.)

J. Thermal Analysis. All thermal analysis measurements were performed under a nitrogen atmosphere at heating and cooling rates of 10 °C/min.

Thermogravimetric Analysis (TGA) was performed on a TA Instruments Q500 TGA on sample sizes of approximately 5 mg between 22 °C and 700 °C.

Differential Scanning Calorimetry (DSC) was performed on a TA Instruments Q1000 Temperature Modulated DSC on sample sizes of approximately 5 mg between -50 °C to 300 °C. Temperature and heat flow calibration was verified via indium, tin, and lead standards at the same heating rate as the samples.

K. Mechanical Property Analyses of the Kapton Seals

Standardized Test Results. By the ASTM-D882-91 testing methodology, the accepted tensile strength and percent elongation of a 5 mil thick FN type Kapton Film are 165 MPa and 50 %, respectively. By this ASTM testing methodology the secant modulus can be as high as 2.6 GPa.

Modulus Test Results. Since the sample size is restricted to 19.1 mm strips of Kapton seal material that have a nominal width of approximately 1 mm mechanical test were performed on an RSA III Dynamic Mechanical Analyzer using the 3500 g Transducer. Each sample was deformed from a nominal gauge length of 5 mm at a rate of 0.05 mm/s for 200 s. Eight reference samples of FN131L material were tested to provide the expected secant modulus at 4 % strain that should be obtained for FN type Kapton Film using this approach.

IV. RESULTS AND DISCUSSION

A. Resistance Measurements. No resistance measurements could be made on BNBR samples. At the request of NHTSA, the resistance measurements are provided for reference purposes only as part of the disassembly process. No analysis is provided. In the following tables, a designation of “open” for the resistance indicates a resistance in excess of 25 GΩ. For an unused switch, the following parameters were obtained:

- Resistance from T1 to T2 = 0.06 Ω
- Resistance from T1 to Ground = open
- Resistance from T2 to Ground = open

Table 2. Resistance Measurements on Likely Bad SCDS

Switch	Resistance (Ω)		
	T1 to T2	T1 to Ground	T2 to Ground
6	-0.036	open	open
30	-0.042	1.4x10 ⁹	6.1x10 ⁹
32	-0.041	5.0x10 ⁹	open
35	-0.047	2.7x10 ⁹	open
61	-0.046	open	open
62	-0.045	no lock	1.1x10 ⁹

Table 3. Resistance Measurements on LBWBF SCDS

Switch	Resistance (Ω)		
	T1 to T2	T1 to Ground	T2 to Ground
4	6.24	810	790
9	2.60x10 ⁵	6.6	8.72x10 ⁵
45	1.16x10 ⁴	1.6x10 ⁴	1.0x10 ⁴
46	2.07	91	23
48	3.3x10 ⁵	3.3x10 ⁴	5.3x10 ⁴
53	1.9x10 ¹	4.4x10 ⁵	2.57x10 ⁵
59	1.1x10 ⁶	3.7x10 ³	1.4x10 ⁶
69	2.7x10 ⁵	3.5x10 ³	5.0x10 ⁷
76	3.2x10 ⁵	3.3x10 ⁵	3.80x10 ⁵
80	6.4x10 ³	5.6x10 ³	132

Table 4. Resistance Measurements on Leaker SCDS

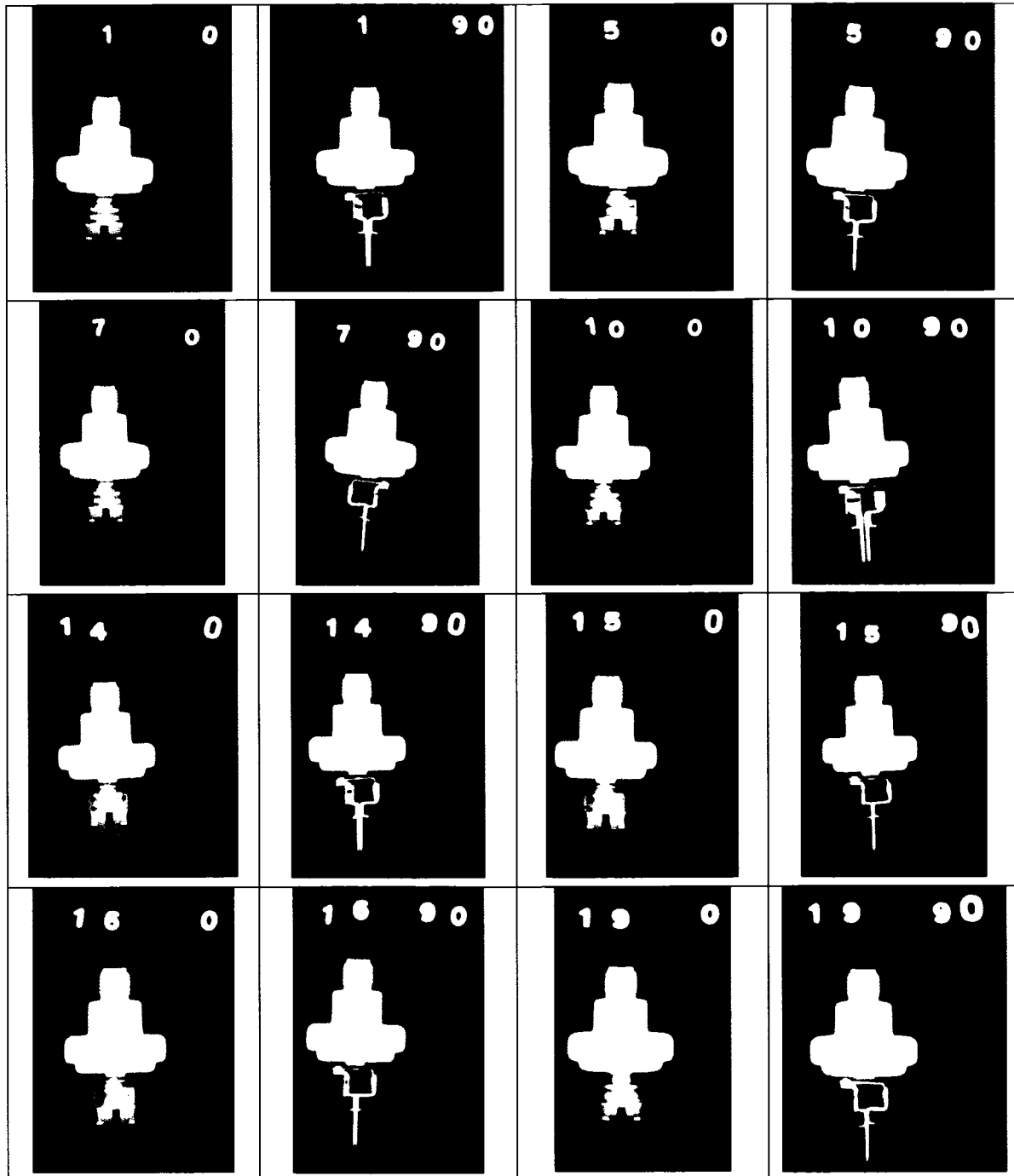
Switch	Resistance (Ω)			Voltage (V)
	T1 to T2	T1 to Ground	T2 to Ground	
3	19.43	43.8	1.18	0.0
17	6.0×10^4	3.6×10^4	4.0×10^4	0.3
17	4.8×10^4	3.7×10^4	4.0×10^4	0
49	137	2.68×10^4	2.48×10^3	0
50	0	open	open	0
52	1.44×10^5	9.2×10^4	7.2×10^4	0.0071
55	6.0×10^5	220	1.9×10^4	-0.2412
56	0.1	4.12×10^4	6.1×10^4	0
57	6.50	4.8×10^6	4.3×10^6	0

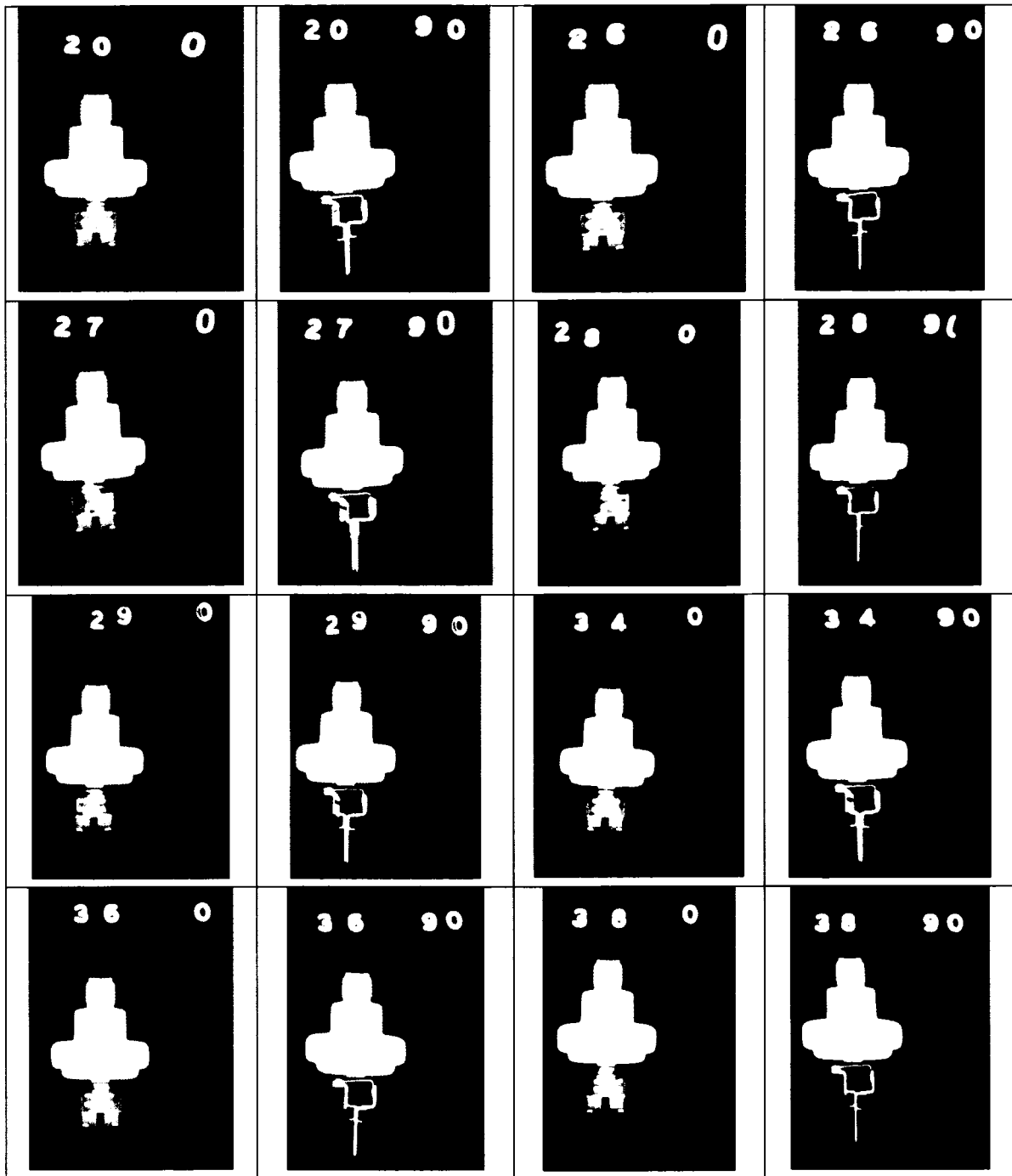
Table 5. Resistance Measurements on Likely Good SCDS

SCDS #	Resistance (Ω)		
	T1 to T2	T1 to Ground	T2 to Ground
1	0.033	open	open
5	0	open	open
7	0.026	1.1×10^9	open
10	-0.013	7.5×10^9	open
14	-0.013	1.06×10^{10}	open
15	-0.018	open	open
16	-0.019	2.2×10^{10}	open
18	-0.026	open	open
19	-0.027	open	open
20	-0.022	open	open
26	-0.023	open	open
27	-0.022	open	open
28	-0.025	open	open
29	-0.023	open	open
34	-0.028	open	open
36	-0.041	open	open
38	-0.032	6.0×10^9	open
40	-0.043	3.7×10^9	open

B. X-ray Photography. At the request of NHTSA, the x-ray photographs are provided for reference purposes only as part of the disassembly process. In Table 6 through Table 10, the x-ray photographs of the SCDS's are provided.

Table 6. X-Ray Photographs of Likely Good SCDS's





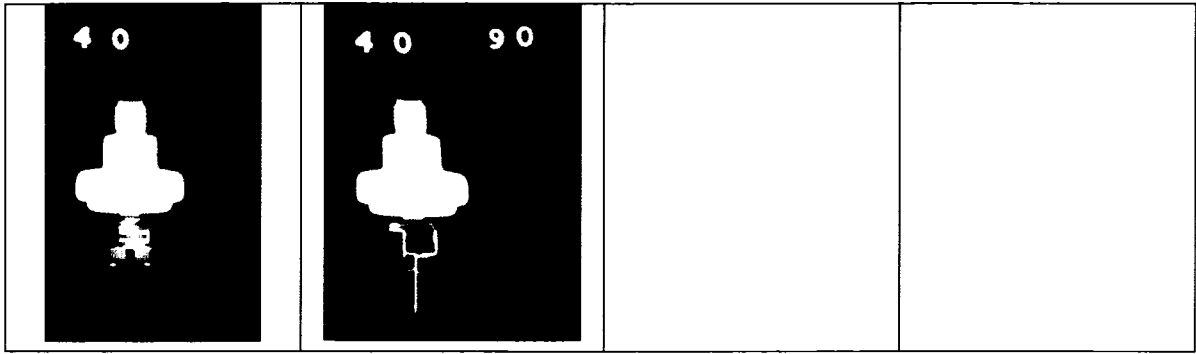


Table 7. X-Ray Photographs of Likely Bad SCDS's












06 0 	06 90 		
32 0 			
61 0 	62 0 	62 90 	

Table 8. X-Ray Photographs of Low Mileage Likely Bad SCDS's

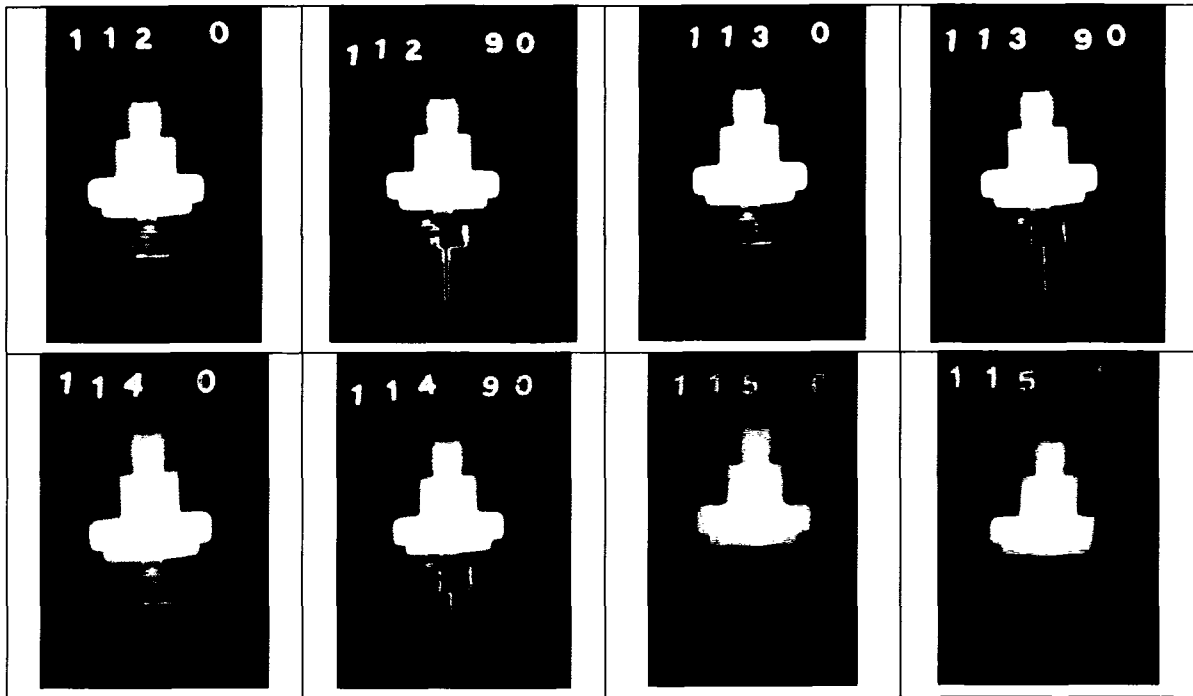


Table 9. X-Ray Photographs of Light Burn with Brake Fluid Remaining SCDS's


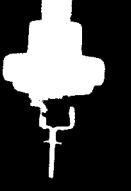















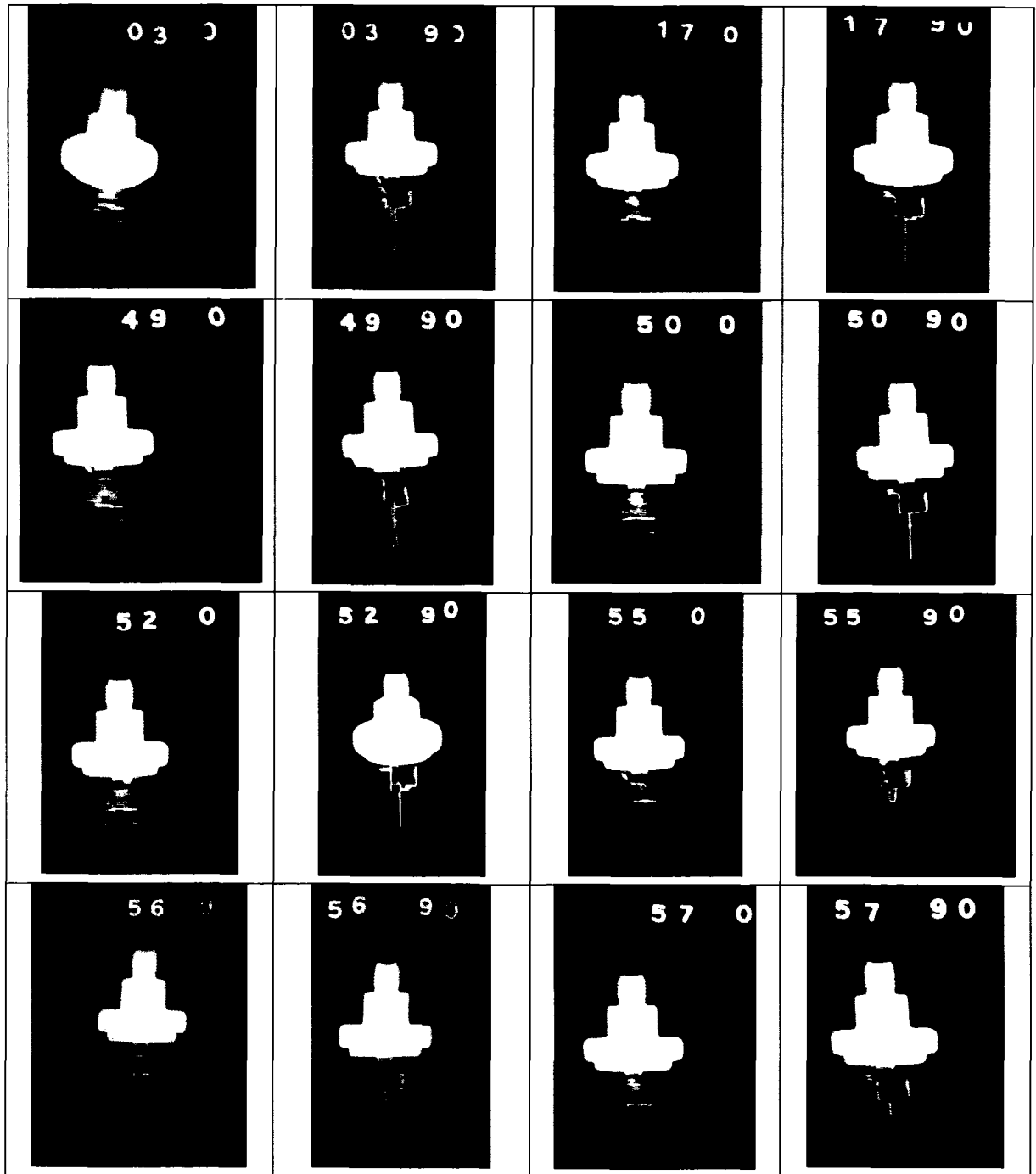
4 0 	4 90 	9 0 	9 90 
45 0 	45 90 	46 90 	
48 0 	48 90 	53 0 	53 90 
69 0 	69 90 	76 0 	76 90 
80 0 	80 90 		

Table 10. X-Ray Photographs of Leaker SCDS's



C. Optical Images of Kapton Seals

In general the Kapton seals from the bad SCDSs were found to have cracks such as those shown in Figure 5. In contrast, the Likely Good specimens were usually found to be devoid of the large cracks found in Figure 5 (see Figure 6 for comparison). However, around the button region of the converter (see Figure 1b) small microcracks were typically found to occur (see Figure 7) in specimens labeled as Likely Good.

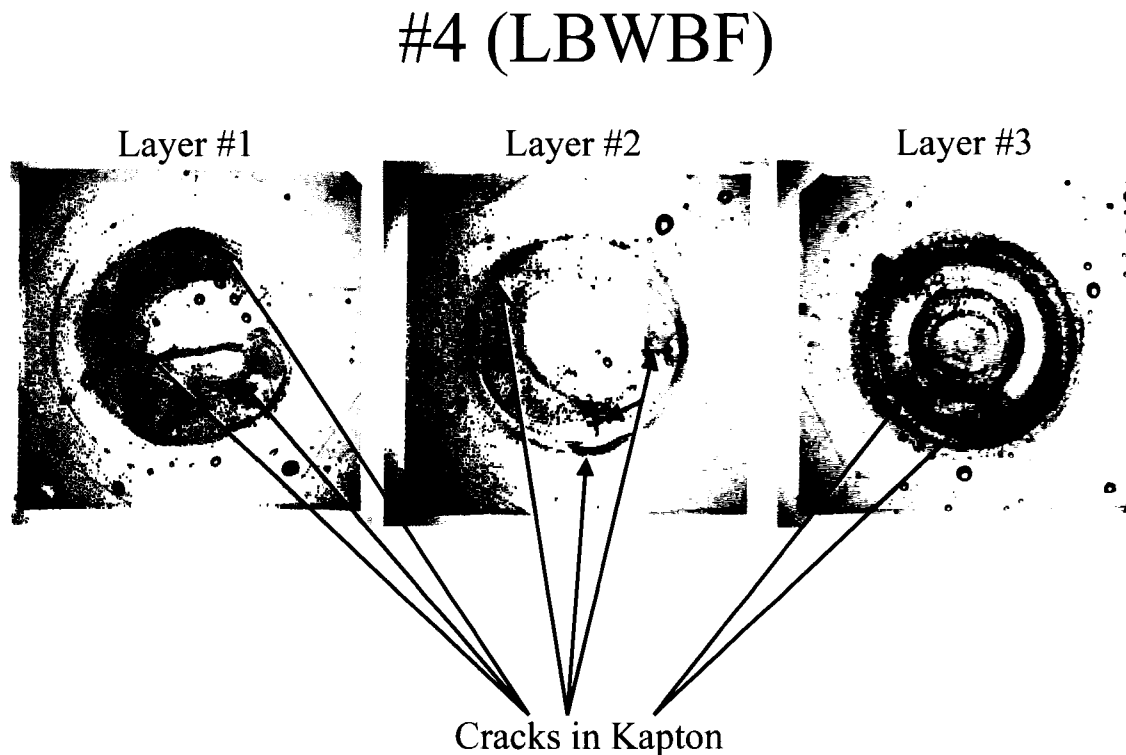


Figure 5. Optical images of Kapton film layers from #4 speed control deactivation switch (SCDS). This SCDS was characterized as a bad device that was lightly burned with brake fluid remaining (LBWBF). Note the cracks in each of the layers. Layer #1 is the film that is next to the brake fluid.

#5 (Likely Good)

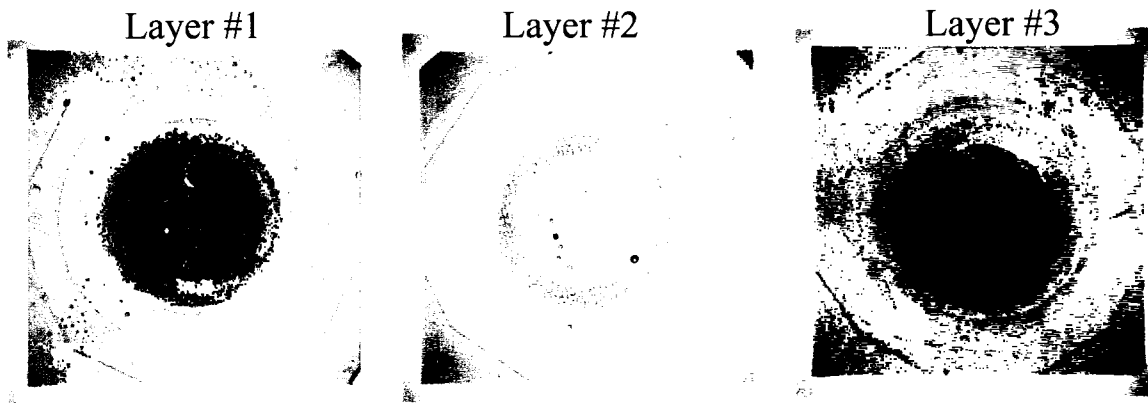


Figure 6. Optical images of Kapton film layers from #5 speed control deactivation switch (SCDS). This SCDS was characterized as a "Likely Good." Note the absence of large cracks in each of the layers. Layer #1 is the film that is next to the brake fluid.

#10 (Likely Good)

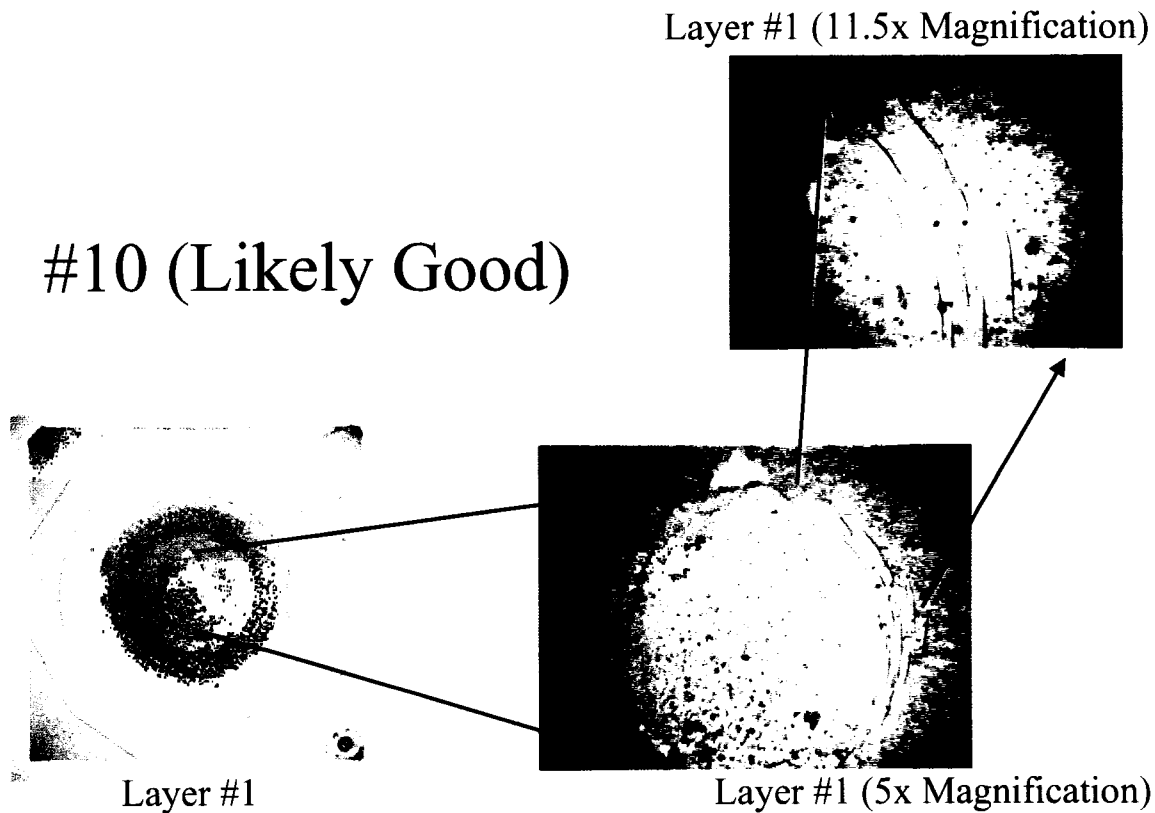
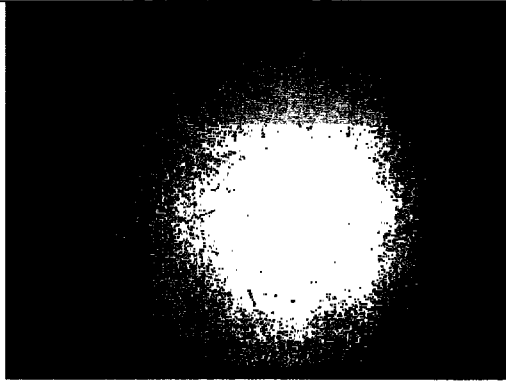
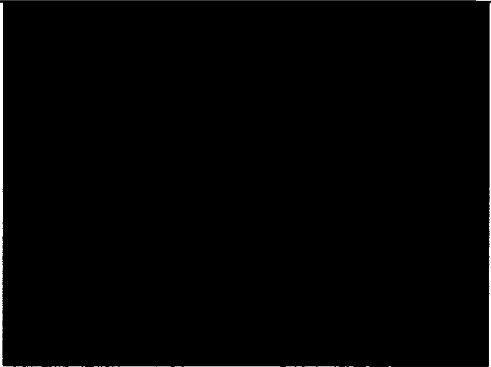
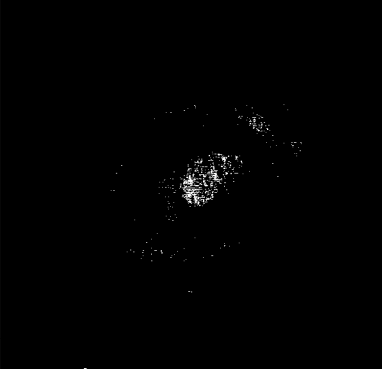


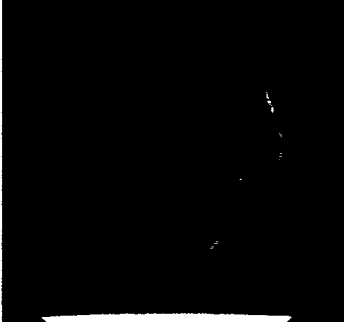


Figure 7. Magnification of region on Kapton film where it is deformed by the button on the converter (see Figure 1). Note circular pattern of cracks.

D. Polarized Optical Microscopy (POM). POM was examined as a potential method for characterizing the orientation and/or stress states of the seals. Color observed for materials between crossed polarizers indicates an orientation in the material; no light is visible if there is no orientation as can be seen for the black regions outside of the material. While deformation patterns were clear between the as-received Kapton-FEP laminate and those of the seals, no pattern of differences could be identified between the different types of switches.

Table 11. Examples Polarized Optical Microscopy Images for Characterization of Orientation

 <p data-bbox="264 961 727 993">As Received Kapton-FEP Laminate</p>	 <p data-bbox="1052 947 1214 978">New Switch</p>
 <p data-bbox="289 1367 701 1398">Likely Good – SCDS 1, Layer 2</p>	 <p data-bbox="922 1356 1344 1388">Likely Good – SCDS 16, Layer 2</p>
 <p data-bbox="191 1755 799 1787">Light Burn w/ Brake Fluid– SCDS 48, Layer 2</p>	 <p data-bbox="928 1738 1334 1770">Likely Bad– SCDS 62, Layer 2</p>

E. Measurescope Imaging.

As the brakes are repeatedly applied and released, the Kapton seals in the SCDS flex between two positions. The first is called the seat position where the seal conforms to the valley region formed by the button on the converter and the washer (see Figure 1b). The conformation of the seal over this region results in the normal wear circular microcracks observed in Figure 7. Theoretical calculations indicate that the seal experiences approximately (3 to 4) % strain in this position. Since this is beyond the strain level for linear viscoelastic behavior this should result in some permanent deformation in the seal.

In the second position, called the open position, the seal is pulled away from the converter button toward the top of the hexport body. In this position the extent of deformation on the seal will depend on the magnitude of the forces pulling the seal into the open position. An example of the seal in the open position is shown in Figure 8, for an SCDS that has been potted in epoxy resin and cut open.



Figure 8. Picture of a cross-sectioned, potted SCDS. Note that the seals are pulled away from the valley formed between the converter button and washer. Compare with Figure 1.

Using an MM-40 Nikon measuring microscope equipped with a 1x magnifying lens, each Kapton seal layer was observed in the reflection mode. A circular white ring was observed on most of the specimens labeled Likely Good, indicating that the seal layer was conforming to the contour of the valley region (see Figure 10). For all specimens labeled Leakers or LBWBF, the circular ring was absent or distorted (see Figure 11 and Figure 12). In each of these specimens evidence of single and multiple teardrop distortions were found on each Kapton seal layer (see Figure 9 below).



Figure 9. Photograph of a teardrop distortion in the Kapton seal.

It is known that the Kapton seal can undergo at least 50 % deformation and that the deformation on the seal in the seat position is only about (3 to 4) % strain. Therefore, the distortion of the circular ring in the bad specimens may be due to extensive permanent deformation occurring on the seal in the open position, slippage of the seal past the gasket when the seal is deformed to the open position, and/or fracture of the seal layer at the gasket seal interface. The first two cases would result in the formation of a teardrop since there would now be excess material in the valley region. Repeated deformations around the teardrop would result in the cracks observed in Figure 5. For completeness all MM-40 images are included in Attachment 2.

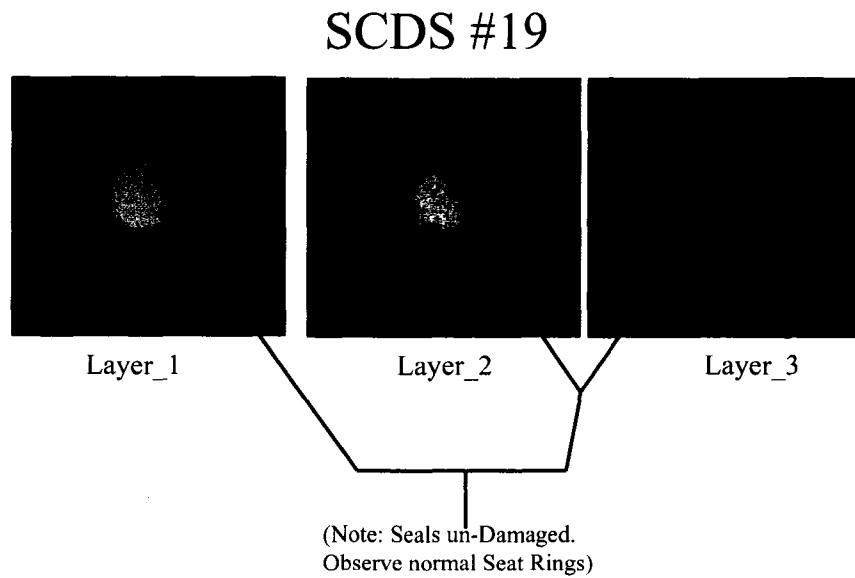


Figure 10. Images of Kapton seal layers of SCDS #19 (Likely Good) taken with MM-40 Nikon measuring microscope. Observed the circular ring in each layer that indicates that the seal is seating properly in the seat position.

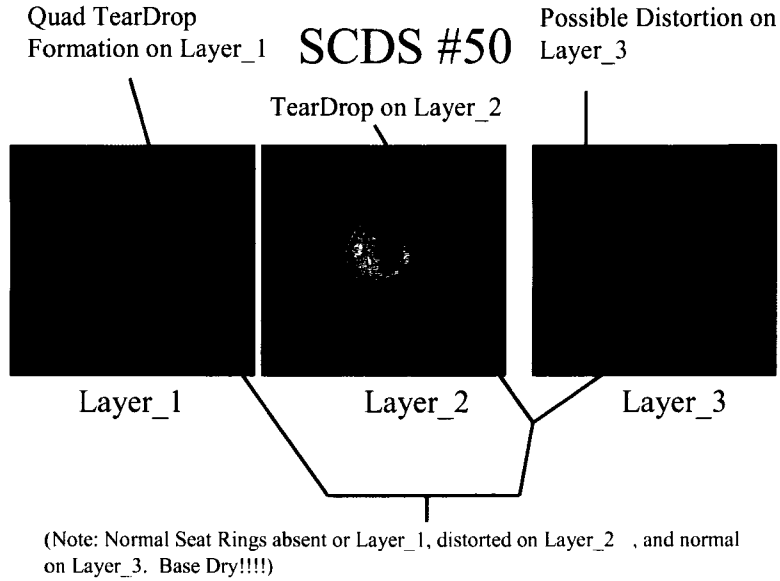


Figure 11. Images of Kapton seal layers of SCDS #50 (Leaker) taken with MM-40 Nikon measuring microscope. Observe distortion of circular ring in each layer.

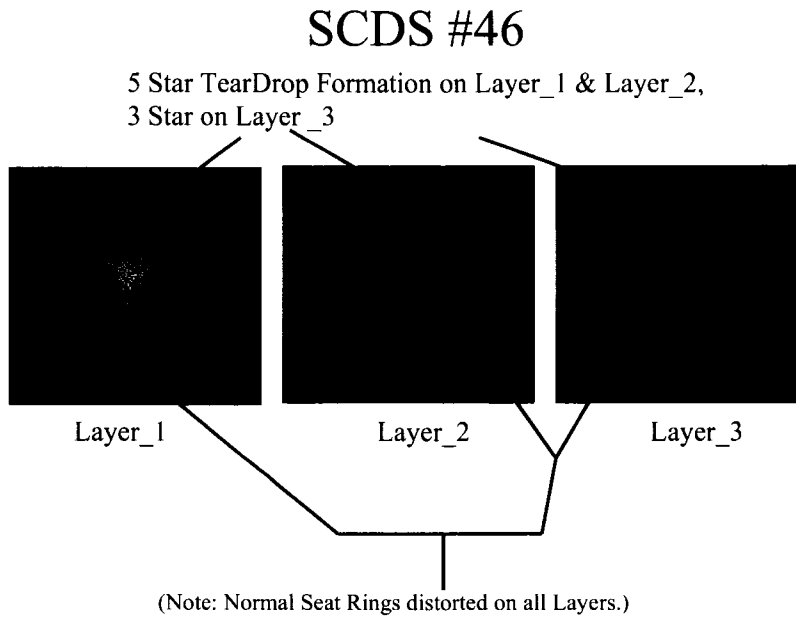


Figure 12. Images of Kapton seal layers of SCDS #46 (LBWBF) taken with MM-40 Nikon measuring microscope. Observe distortion or absence of circular ring in each layer.

F. Electron Microscopy.

The samples were imaged using a Hitachi S-4700-II field emission-scanning electron microscope (FE-SEM) equipped with a x-ray microanalysis for elemental analysis. The samples were gold (Au) coated prior to imaging to reduce charging. Using the FE-SEM cracked or compromised regions of the sample were identified and imaged. The exterior and interior of a crack were analyzed for differences in chemical components. Similar features were seen on samples investigated (SCDS #4 – bad LBWBF, SCDS #7 – likely good) and the x-ray microanalysis indicated a fluorine rich outer layer (surface) and a oxygen rich inner layer (crack) at the crack sights, but there was no evidence of nitrogen on the inner surfaces. On both samples a peak at approximately 2200 eV was present. This was unexpected and may be a result of a contaminant, most likely Na, Zn, or Cu, from automotive fluids. The SEM and x-ray microanalysis failed to demonstrate any significant differences between the LBWBF and Likely Good SCDS examined.



Figure 13. TEM Image of Damage Regions on SCDS# 4

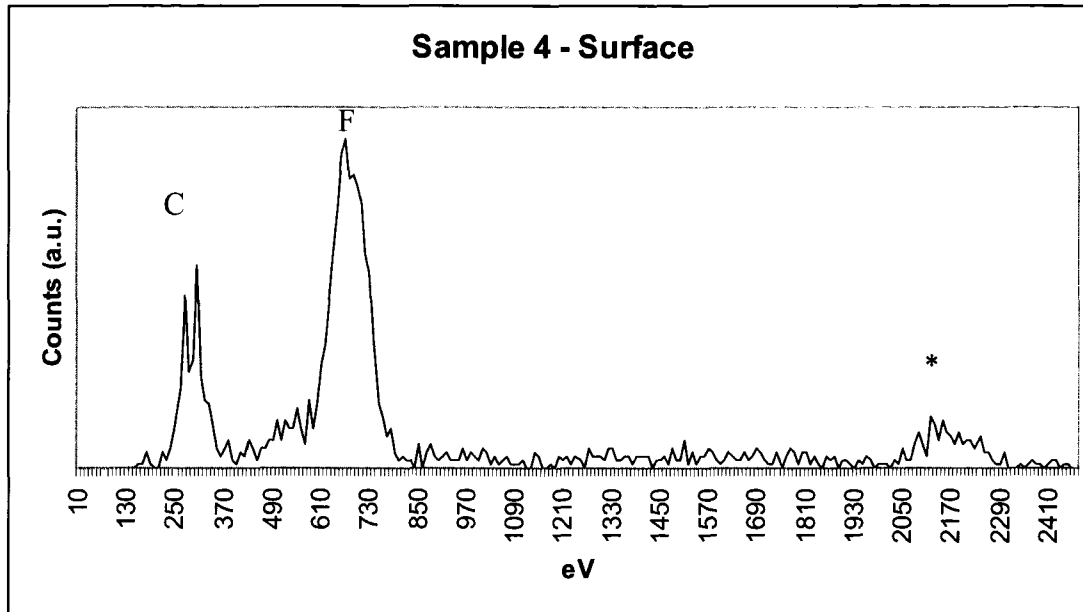


Figure 14. X-ray microanalysis of SCDS #4, Surface, * This peak was not expected, possibly a contaminant, possible matches are Na, Cu, Zn

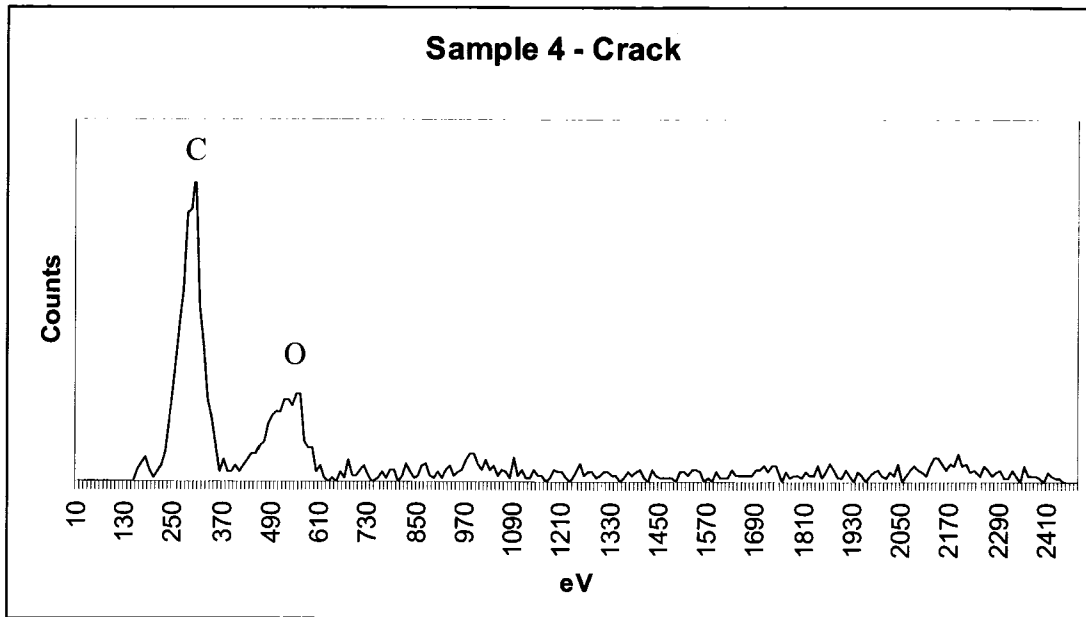


Figure 15. X-ray microanalysis of SCDS #4, Crack

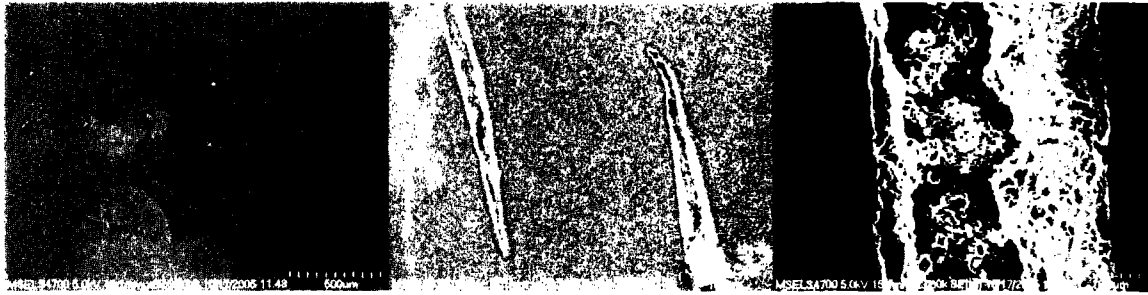


Figure 16. TEM micrographs of damage regions on SCDS #7.

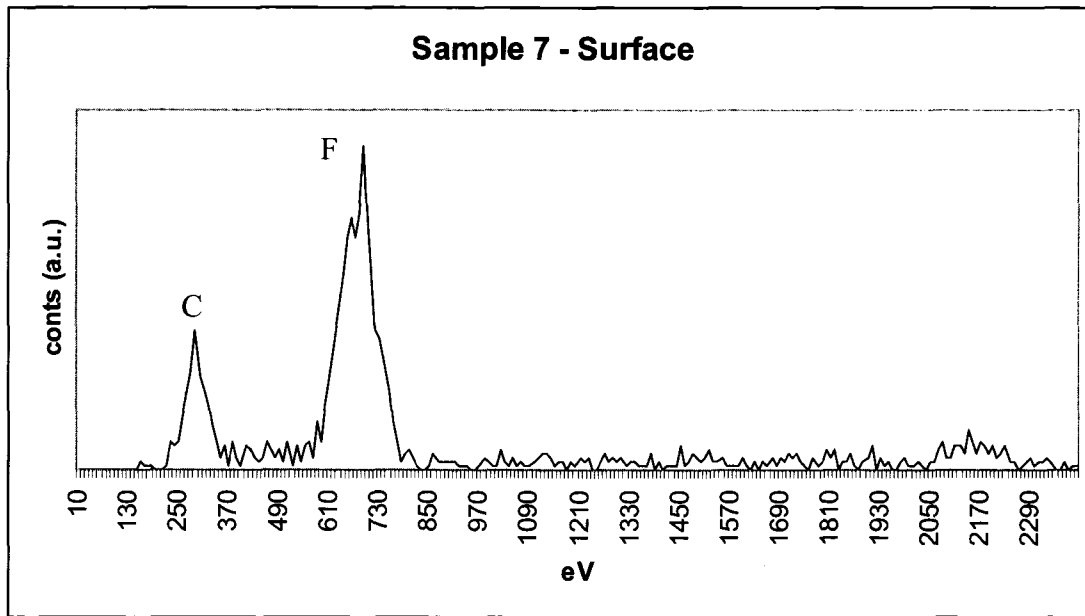


Figure 17. X-ray microanalysis of SCDS #7, Surface

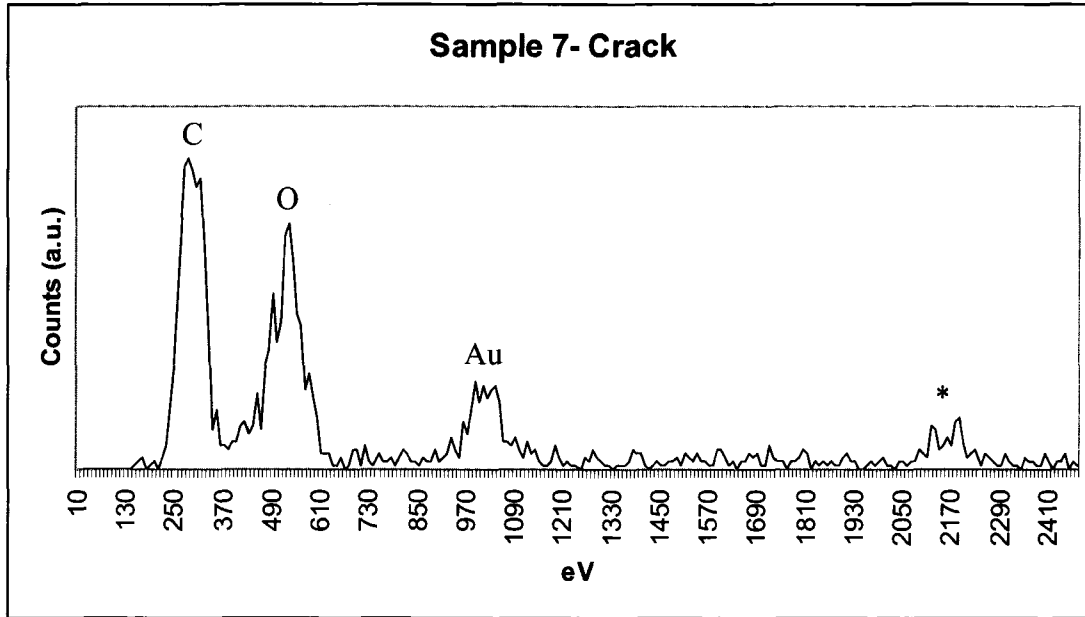


Figure 18. X-ray microanalysis of SCDS #7, Crack, * This peak was not expected, possibly a contaminant, possible matches are Na, Cu, Zn

G. Dimensional Analyses.

(1) *Thickness Measurements.* Table 12 through Table 17 display the results of the thickness measurements on the Kapton/FEP seals. Note that in each of the tables, **bold text** indicates a minimum or maximum of a quantity for a given category of SCDS. Table 12 provides information regarding the variation in thickness due to the crimping procedure for Likely Good, an Unused SCDS, LBWBF, and BWBF, as each measurement is the average of 14 separate measurements throughout the crimped and uncrimped regions. The range of relative deviation in thickness between the categories overlapped, with BWBR ranging between 1.6 % and 21.5 %, LBWBF between 1.1 % and 9.2 %, and Unused and Likely Good ranging between 0.8 % and 5.2 %. The high deviations for the switches that underwent some burning (LBWBF and BWBR) are to be expected since the samples were physically distorted by the heat. Table 13 through Table 17 are the results of measurements at each of the four corners of the SCDS seals. The average, standard deviation, and relative deviation are provided for each of the layers measured. (Values are also provided for the maximum deviation in thickness, i.e., the difference between the point with the maximum thickness and the point with the minimum thickness within a given Kapton/FEP seal.) Comparison of Likely Good, Likely Bad, and Leaker seals shows no correlation. Likely Good ranges from 0.5 % to 4.1 % relative deviation in thickness, versus 0.4 % to 2.6 % for Likely Bad and 0.6 % to 4.2 % for Leakers. From these data, there is no obvious correlation between thickness variations and SCDS failure behavior.

Table 12. Analysis of Thickness Variations Due to Crimping Process

Category	SCDS #	Layer #	Average (mm)	Std Dev (mm)	Rel Dev
Likely Good	5	1	0.1250	0.0011	0.9%
Likely Good	5	2	0.1221	0.0024	2.0%
Likely Good	5	3	0.1227	0.0021	1.7%
Likely Good	7	1	0.1258	0.0021	1.7%
Likely Good	7	2	0.1232	0.0023	1.8%
Likely Good	7	3	0.1249	0.0010	0.8%
Likely Good	10	1	0.1249	0.0014	1.1%
Likely Good	10	2	0.1252	0.0013	1.0%
Likely Good	10	3	0.1248	0.0013	1.0%
Likely Good	14	1	0.1222	0.0018	1.4%
Likely Good	14	2	0.1225	0.0011	0.9%
Likely Good	14	3	0.1256	0.0018	1.4%
Likely Good	15	1	0.1232	0.0014	1.2%
Likely Good	15	2	0.1250	0.0027	2.2%
Likely Good	15	3	0.1275	0.0066	5.2%
Likely Good	16	1	0.1213	0.0017	1.4%
Likely Good	16	2	0.1214	0.0016	1.4%
Likely Good	16	3	0.1250	0.0016	1.2%
Likely Good	18	1	0.1211	0.0018	1.5%
Likely Good	18	2	0.1254	0.0016	1.3%
Likely Good	18	3	0.1215	0.0013	1.1%
Unused Sensor		1	0.1270	0.0015	1.2%
Unused Sensor		2	0.1267	0.0021	1.6%
Unused Sensor		3	0.1257	0.0015	1.2%
LBWBF	4	1	0.1237	0.0027	2.2%
LBWBF	4	2	0.1264	0.0014	1.1%
LBWBF	4	3	0.1252	0.0030	2.4%
LBWBF	9	1	0.1279	0.0024	1.9%
LBWBF	9	2	0.1227	0.0031	2.5%
LBWBF	9	3	0.1277	0.0079	6.2%
LBWBF	48	1	0.1260	0.0071	5.6%
LBWBF	48	2	0.1250	0.0030	2.4%
LBWBF	48	3	0.1295	0.0119	9.2%
BWBR	51	1	0.0777	0.0040	5.2%
BWBR	51	2	0.0821	0.0085	10.4%
BWBR	51	3	0.0850	0.0154	18.1%
BWBR	60	1	0.0779	0.0063	8.1%
BWBR	60	2	0.0893	0.0192	21.5%
BWBR	60	3	0.0808	0.0066	8.1%
BWBR	65	1	0.1216	0.0039	3.2%
BWBR	65	2	0.1227	0.0024	2.0%
BWBR	65	3	0.1264	0.0052	4.1%
BWBR	75	1	0.1273	0.0025	2.0%
BWBR	75	2	0.1299	0.0020	1.6%
BWBR	75	3	0.1266	0.0027	2.2%

Table 13. Analysis of Thickness Variation in Likely Good and Unused SCDS's

Category	SCDS #	Layer #	Average (mm)	Std Dev (mm)	Rel Dev	Max - Min (mm)
Likely Good	1	1	0.1217	0.0010	0.8%	0.0022
Likely Good	1	2	0.1209	0.0013	1.1%	0.0026
Likely Good	1	3	0.1212	0.0010	0.8%	0.0022
Likely Good	5	1	0.1236	0.0005	0.4%	0.0011
Likely Good	5	2	0.1202	0.0041	3.4%	0.0087
Likely Good	5	3	0.1205	0.0027	2.2%	0.0065
Likely Good	7	1	0.1237	0.0030	2.4%	0.0067
Likely Good	7	2	0.1204	0.0025	2.1%	0.0059
Likely Good	7	3	0.1238	0.0004	0.3%	0.0009
Likely Good	10	1	0.1234	0.0020	1.6%	0.0042
Likely Good	10	2	0.1247	0.0010	0.8%	0.0024
Likely Good	10	3	0.1237	0.0010	0.8%	0.0021
Likely Good	14	1	0.1204	0.0024	2.0%	0.0052
Likely Good	14	2	0.1214	0.0009	0.8%	0.0021
Likely Good	14	3	0.1240	0.0013	1.0%	0.0027
Likely Good	15	1	0.1213	0.0010	0.8%	0.0021
Likely Good	15	2	0.1226	0.0010	0.8%	0.0021
Likely Good	15	3	0.1240	0.0008	0.7%	0.0017
Likely Good	16	1	0.1190	0.0014	1.1%	0.0030
Likely Good	16	2	0.1195	0.0012	1.0%	0.0028
Likely Good	16	3	0.1233	0.0012	1.0%	0.0027
Likely Good	18	1	0.1206	0.0032	2.6%	0.0065
Likely Good	18	2	0.1239	0.0022	1.8%	0.0045
Likely Good	18	3	0.1208	0.0009	0.7%	0.0020
Likely Good	19	1	0.1200	0.0022	1.9%	0.0052
Likely Good	19	2	0.1261	0.0010	0.8%	0.0024
Likely Good	19	3	0.1264	0.0008	0.6%	0.0016
Likely Good	20	1	0.1252	0.0011	0.9%	0.0028
Likely Good	20	2	0.1203	0.0014	1.2%	0.0027
Likely Good	20	3	0.1259	0.0006	0.5%	0.0013

Table 13 cont'd.

Category	SCDS #	Layer #	Average (mm)	Std Dev (mm)	Rel Dev	Max - Min (mm)
Likely Good	26	1	0.1197	0.0049	4.1%	0.0109
Likely Good	26	2	0.1213	0.0008	0.7%	0.0019
Likely Good	26	3	0.1230	0.0008	0.7%	0.0016
Likely Good	27	1	0.1255	0.0014	1.1%	0.0032
Likely Good	27	2	0.1242	0.0007	0.6%	0.0016
Likely Good	27	3	0.1247	0.0018	1.4%	0.0038
Likely Good	28	1	0.1207	0.0013	1.0%	0.0028
Likely Good	28	2	0.1234	0.0006	0.5%	0.0015
Likely Good	28	3	0.1200	0.0016	1.3%	0.0037
Likely Good	29	1	0.1228	0.0015	1.2%	0.0032
Likely Good	29	2	0.1200	0.0017	1.5%	0.0039
Likely Good	29	3	0.1222	0.0023	1.9%	0.0053
Likely Good	34	1	0.1255	0.0022	1.7%	0.0053
Likely Good	34	2	0.1248	0.0027	2.1%	0.0065
Likely Good	34	3	0.1255	0.0024	1.9%	0.0057
Likely Good	36	1	0.1232	0.0015	1.3%	0.0036
Likely Good	36	2	0.1182	0.0027	2.3%	0.0064
Likely Good	36	3	0.1210	0.0011	0.9%	0.0024
Likely Good	38	1	0.1225	0.0022	1.8%	0.0045
Likely Good	38	2	0.1257	0.0025	2.0%	0.0060
Likely Good	38	3	0.1233	0.0027	2.2%	0.0062
Likely Good	40	1	0.1229	0.0019	1.5%	0.0046
Likely Good	40	2	0.1227	0.0028	2.3%	0.0064
Likely Good	40	3	0.1217	0.0009	0.8%	0.0021
Unused Sensor		1	0.1263	0.0026	2.1%	0.0054
Unused Sensor		2	0.1246	0.0028	2.2%	0.0062
Unused Sensor		3	0.1245	0.0019	1.5%	0.0041

Table 14. Analysis of Thickness Variation in Likely Bad SCDS's

Category	SCDS #	Layer #	Average (mm)	Std Dev (mm)	Rel Dev	Max - Min (mm)
Likely Bad	6	1	0.1195	0.0031	2.6%	0.0058
Likely Bad	6	2	0.1250	0.0011	0.9%	0.0024
Likely Bad	6	3	0.1228	0.0003	0.2%	0.0006
Likely Bad	30	1	0.1232	0.0010	0.8%	0.0022
Likely Bad	30	2	0.1217	0.0009	0.8%	0.0018
Likely Bad	30	3	0.1228	0.0010	0.9%	0.0025
Likely Bad	32	1	0.1187	0.0012	1.0%	0.0022
Likely Bad	32	2	0.1204	0.0010	0.8%	0.0019
Likely Bad	32	3	0.1225	0.0004	0.4%	0.0010
Likely Bad	35	1	0.1190	0.0026	2.2%	0.0056
Likely Bad	35	2	0.1220	0.0027	2.2%	0.0049
Likely Bad	35	3	0.1205	0.0005	0.4%	0.0011
Likely Bad	61	1	0.1214	0.0040	3.3%	0.0092
Likely Bad	61	2	0.1231	0.0018	1.4%	0.0041
Likely Bad	61	3	0.1186	0.0021	1.8%	0.0047
Likely Bad	62	1	0.1230	0.0013	1.1%	0.0032
Likely Bad	62	2	0.1220	0.0014	1.2%	0.0035
Likely Bad	62	3	0.1191	0.0009	0.8%	0.0022

Table 15. Analysis of Thickness Variation in Leaker SCDS's

Category	SCDS #	Layer #	Average (mm)	Std Dev (mm)	Rel Dev	Max - Min (mm)
Leaker	3	1	0.1200	0.0005	0.4%	0.0011
Leaker	3	2	0.1186	0.0050	4.2%	0.0115
Leaker	3	3	0.1192	0.0031	2.6%	0.0069
Leaker	17	1	0.1223	0.0019	1.6%	0.0040
Leaker	17	2	0.1207	0.0024	2.0%	0.0056
Leaker	17	3	0.1222	0.0011	0.9%	0.0024
Leaker	49	1	0.1201	0.0027	2.3%	0.0065
Leaker	49	2	0.1219	0.0020	1.6%	0.0046
Leaker	49	3	0.1206	0.0026	2.1%	0.0060
Leaker	50	1	0.1236	0.0029	2.3%	0.0062
Leaker	50	2	0.1203	0.0037	3.1%	0.0079
Leaker	50	3	0.1230	0.0024	1.9%	0.0053
Leaker	52	1	0.1225	0.0027	2.2%	0.0061
Leaker	52	2	0.1183	0.0019	1.6%	0.0044
Leaker	52	3	0.1229	0.0012	0.9%	0.0024
Leaker	55	1	0.1239	0.0008	0.6%	0.0016
Leaker	55	2	0.1239	0.0012	1.0%	0.0027
Leaker	55	3	0.1212	0.0029	2.4%	0.0063
Leaker	56	1	0.1180	0.0047	4.0%	0.0109
Leaker	56	2	0.1228	0.0016	1.3%	0.0036
Leaker	56	3	0.1203	0.0045	3.8%	0.0102
Leaker	57	1	0.1213	0.0030	2.5%	0.0064
Leaker	57	2	0.1208	0.0019	1.6%	0.0043
Leaker	57	3	0.1184	0.0027	2.3%	0.0061

Table 16. Analysis of Thickness Variation in LBWBF SCDS's

Category	SCDS #	Layer #	Average (mm)	Std Dev (mm)	Rel Dev	Max - Min (mm)
LBWBF	4	1	0.1216	0.0012	1.0%	0.0025
LBWBF	4	2	0.1248	0.0005	0.4%	0.0011
LBWBF	4	3	0.1216	0.0012	1.0%	0.0029
LBWBF	9	1	0.1251	0.0016	1.3%	0.0034
LBWBF	9	2	0.1197	0.0020	1.7%	0.0046
LBWBF	9	3	0.1207	0.0011	0.9%	0.0020
LBWBF	45	1	0.1252	0.0014	1.1%	0.0027
LBWBF	45	2	0.1244	0.0033	2.7%	0.0077
LBWBF	45	3	0.1177	0.0036	3.0%	0.0079
LBWBF	46	1	0.1278	0.0183	14.3%	0.0385
LBWBF	46	2	0.1097	0.0176	16.0%	0.0345
LBWBF	46	3	0.1468	0.0352	23.9%	0.0748
LBWBF	48	1	0.1198	0.0018	1.5%	0.0043
LBWBF	48	2	0.1222	0.0014	1.2%	0.0032
LBWBF	48	3	0.1214	0.0030	2.4%	0.0063
LBWBF	53	1	0.1246	0.0013	1.1%	0.0025
LBWBF	53	2	0.1246	0.0015	1.2%	0.0037
LBWBF	53	3	0.1225	0.0017	1.4%	0.0041
LBWBF	59	1	0.1213	0.0022	1.8%	0.0049
LBWBF	59	2	0.1226	0.0021	1.7%	0.0049
LBWBF	59	3	0.1234	0.0015	1.2%	0.0035
LBWBF	69	1	0.1200	0.0002	0.2%	0.0005
LBWBF	69	2	0.1179	0.0021	1.8%	0.0052
LBWBF	69	3	0.1202	0.0035	2.9%	0.0067
LBWBF	76	1	0.1226	0.0021	1.7%	0.0047
LBWBF	76	2	0.1218	0.0039	3.2%	0.0085
LBWBF	76	3	0.1236	0.0012	1.0%	0.0028
LBWBF	80	1	0.1231	0.0011	0.9%	0.0024
LBWBF	80	2	0.1237	0.0033	2.6%	0.0080
LBWBF	80	3	0.1231	0.0023	1.9%	0.0055

Table 17. Analysis of Thickness Variation in BWBR SCDS's

Category	SCDS #	Layer #	Average (mm)	Std Dev (mm)	Rel Dev	Max - Min (mm)
BWBR	51	1	0.0743	0.0025	3.4%	0.0054
BWBR	51	2	0.0763	0.0014	1.8%	0.0033
BWBR	51	3	0.0745	0.0012	1.7%	0.0027
BWBR	60	1	0.0740	0.0024	3.2%	0.0053
BWBR	60	2	0.0743	0.0021	2.8%	0.0050
BWBR	60	3	0.0755	0.0008	1.0%	0.0014
BWBR	65	1	0.1170	0.0048	4.1%	0.0112
BWBR	65	2	0.1197	0.0028	2.3%	0.0068
BWBR	65	3	0.1222	0.0022	1.8%	0.0053
BWBR	68	1	0.0924	0.0132	14.3%	0.0266
BWBR	68	2	0.0933	0.0097	10.4%	0.0208
BWBR	68	3	0.0876	0.0011	1.2%	0.0026
BWBR	70	1	0.0756	0.0018	2.3%	0.0038
BWBR	70	2	0.0739	0.0004	0.6%	0.0010
BWBR	70	3	0.0763	0.0030	3.9%	0.0054
BWBR	75	1	0.1242	0.0019	1.5%	0.0046
BWBR	75	2	0.1283	0.0020	1.6%	0.0038
BWBR	75	3	0.1245	0.0038	3.1%	0.0084

(2) *Laminate Layer Thickness Verification.* Figure 19 shows the cross section images of the as-received Kapton laminate, a LBWBF SCDS, and a Likely Good SCDS. The dark bars are the FEP and the region between them is the Kapton. Within the resolution of the technique, there is no apparent difference in the layer thicknesses.

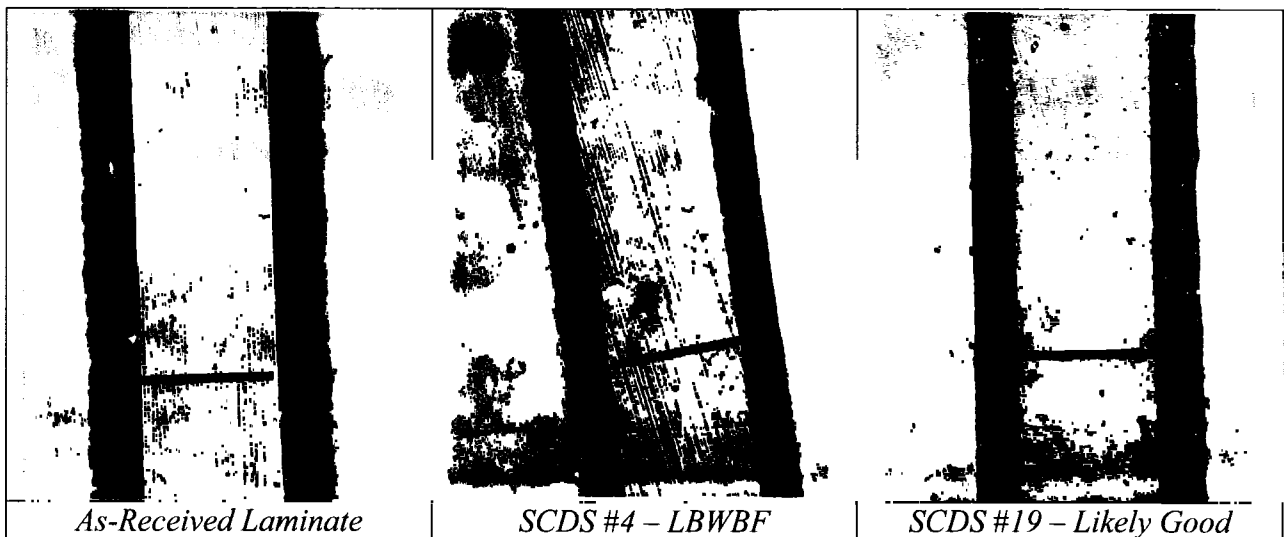


Figure 19. Comparison of FEP (Blue Line) and Kapton (Red Line) Layer Thicknesses Between Samples. Note that the red and blue lines are the same size in each image.

(3) *Switch Dimensions*. The results of the SCDS part dimensions are given in Table 18. For each measurement within a given category of SCDS, the maximum and minimum values are given in **bold text**. The mean and standard deviation of all replicates are given in blue text.

Table 18. Comparison of SCDS Dimensions

Category	SCDS #	Gasket Seat Depth (mm)	Outside Ring Thickness (mm)	Washer Thickness (mm)	O-Ring Thickness (mm)
Likely Good	1	0.67±0.03	2.54±0.09	2.55±0.01	0.71±0.02
Likely Good	5	0.59±0.01	2.47±0.02	2.51±0.02	0.69±0.02
Likely Good	7	0.68±0.01	2.53±0.06	2.49±0.03	0.78±0.03
Likely Good	10	0.62±0.01	2.53±0.06	2.52±0.00	0.78±0.03
Likely Good	14	0.61±0.01	2.59±0.05	2.47±0.01	0.74±0.02
Likely Good	15	0.66±0.01	2.52±0.06	2.51±0.00	0.74±0.03
Likely Good	16	0.65±0.02	2.53±0.03	2.51±0.01	0.73±0.02
Likely Good	18	0.63±0.01	2.60±0.01	2.52±0.00	0.74±0.02
Likely Good	19	0.66±0.02	2.62±0.03	2.50±0.01	0.76±0.01
Likely Good	20	0.65±0.03	2.56±0.03	2.50±0.00	0.75±0.03
Likely Good	26	0.59±0.05	2.66±0.02	2.54±0.02	0.74±0.03
Likely Good	27	0.67±0.01	2.58±0.08	2.50±0.01	0.73±0.04
Likely Good	28	0.64±0.03	2.50±0.03	2.50±0.02	0.74±0.03
Likely Good	29	0.68±0.06	2.55±0.01	2.53±0.00	0.75±0.04
Likely Good	34	0.66±0.01	2.61±0.03	2.49±0.01	0.76±0.02
Likely Good	36	0.66±0.01	2.59±0.06	2.47±0.01	0.71±0.02
Likely Good	38	0.64±0.02	2.48±0.01	2.49±0.02	0.76±0.02
Likely Good	40	0.63±0.01	2.58±0.04	2.53±0.02	0.76±0.01
	Mean	0.67±0.02	2.54±0.08	2.53±0.04	0.74±0.03
Leaker	3	0.67±0.02	2.59±0.04	2.55±0.03	0.75±0.02
Leaker	17	0.64±0.02	2.50±0.02	2.48±0.01	0.78±0.02
Leaker	49	0.66±0.01	2.60±0.08	2.58±0.03	0.73±0.02
Leaker	50	0.70±0.01	2.62±0.12	2.50±0.01	0.68±0.01
Leaker	52	0.66±0.00	2.49±0.04	2.52±0.01	0.74±0.02
Leaker	55	0.69±0.02	2.55±0.05	2.56±0.01	0.76±0.01
Leaker	57	0.64±0.01	2.47±0.01	2.50±0.03	0.73±0.02
	Mean	0.64±0.03	2.56±0.06	2.51±0.02	0.74±0.03
LBWBF	4	0.66±0.01	2.45±0.04	2.51±0.02	0.75±0.04
LBWBF	9	0.66±0.02	2.53±0.08	2.53±0.01	0.73±0.01
LBWBF	46	0.68±0.04	2.50±0.04	2.49±0.01	0.71±0.02
LBWBF	48	0.63±0.00	2.55±0.04	2.48±0.01	0.74±0.01
LBWBF	53	0.67±0.01	2.51±0.01	2.54±0.01	0.76±0.02
LBWBF	59	0.63±0.01	2.51±0.07	2.49±0.01	0.76±0.00
LBWBF	69	0.67±0.01	2.51±0.05	2.52±0.01	0.73±0.01
LBWBF	76	0.68±0.02	2.50±0.01	2.51±0.01	0.76±0.01
LBWBF	80	0.67±0.02	2.50±0.02	2.56±0.02	0.73±0.02
	Mean	0.66±0.02	2.50±0.04	2.51±0.03	0.74±0.02

The average for each of the three categories were the same within the experimental uncertainty. From these data, there is no obvious correlation between switch dimensions and SCDS failure behavior.

H. Density.

The results of the density measurements are given in Table 19. The average for each of the three categories were the same within the experimental uncertainty. From these data, there is no obvious correlation between seal density and SCDS failure behavior.

Table 19. Comparison of Kapton Laminate Seal Densities

SCDS #	Category	Mean Density (g/cm ³)	Std. Dev. (g/cm ³)	Category Mean (g/cm ³)	Category Std. Dev. (g/cm ³)
1	Likely Good	1.737	0.014	1.76	0.04
5	Likely Good	1.738	0.025		
7	Likely Good	1.739	0.0003		
10	Likely Good	1.756	0.0001		
14	Likely Good	1.754	0.020		
15	Likely Good	1.824	0.067		
16	Likely Good	1.750	0.036		
18	Likely Good	1.749	0.047		
19	Likely Good	1.819	0.061		
20	Likely Good	1.755	0.078		
26	Likely Good	1.738	0.013		
27	Likely Good	1.748	0.024		
28	Likely Good	1.822	0.059		
29	Likely Good	1.686	0.040		
34	Likely Good	1.713	0.017		
36	Likely Good	1.750	0.026		
38	Likely Good	1.744	0.0001		
40	Likely Good	1.796	0.070		
3	Leaker	1.594	0.081	1.69	0.06
17	Leaker	1.686	0.016		
49	Leaker	1.688	0.053		
50	Leaker	1.734	0.014		
52	Leaker	1.738	0.016		
55	Leaker	1.722	0.005		
56	Leaker	1.735	0.010		
57	Leaker	1.609	0.096		
4	LBWBF	1.732	0.002	1.73	0.03
9	LBWBF	1.747	0.015		
45	LBWBF	1.695	0.015		
46	LBWBF	1.665	0.002		
48	LBWBF	1.744	0.039		
53	LBWBF	1.748	0.019		
59	LBWBF	1.755	0.003		
69	LBWBF	1.733	0.022		
70	LBWBF	1.742	0.035		
80	LBWBF	1.754	0.040		

I. Infrared Analysis of Material.

The film sandwiches from layer 2 were analyzed using Fourier transform infrared microscopy (Nicolet Magna 550 spectrometer, Nic-Plan microscope) for chemical information relating to film defects. Reflection spectra were taken using a 32X objective and 64 scans. Because of a sinusoidal baseline in the spectra, no correlation could be made between the Likely Good, Likely Bad, and LBWBF samples. This baseline is an artifact of interference of the infrared light and is a common occurrence in infrared spectra of films. This baseline problem made it very difficult to follow subtle changes in peak position and intensity. Gross differences in spectra are only observed in one film where a spectrum was taken in a region of visible damage (Figure 24).

Spectra are grouped as follows: The first group of spectra was taken on the side of the film that was “button up,” the second group was taken on the “button down” side. A spectrum of as-received Kapton (500FN131L) is always included for comparison. The peaks that are labeled are common to all spectra. The optical images to the right of the spectra show the area from which the spectrum was collected. The optical images measure 465 μm by 625 μm .

The peak assignments for the spectra are as follows:

Peak Position (cm^{-1})	Vibrational Assignment
1769	Symmetric C=O stretch (Kapton)
1717	Asymmetric C=O stretch (Kapton)
1504	Benzene ring stretching (Kapton)
1374	Imide C-N-C stretching (Kapton)
1214	Asymmetric C-O-C stretching (kapton)
1152	Symmetric C-O-C stretching (Kapton)
1280 to 1120	CF ₂ Stretch (FEP)

Figure 20 shows the reflectance spectra of the “likely good” Kapton film. Arrows indicate the interference fringes in the baseline, which only grow stronger as wavenumbers decrease and affect the intensity of the absorption peaks. Any differences in intensity of the Kapton peaks among the films in Figure 21 cannot be attributed to differences in the amount of Kapton for the reason discussed above. The same can be concluded for Figure 22 and Figure 23. An image of visible damage is shown optically (bottom image) in Figure 24 for a likely good film sandwich. There are no conclusive chemical differences between the spectrum damaged area and the undamaged Kapton reference film. Figure 25 addresses inspecting damaged and undamaged areas within the same optical image. The Kapton peaks from Area 2 are substantially lower than Area 1 or the Kapton reference film. This is the only instance where we have detected removal of the Kapton with confidence. We also took spectra of the “button down” side of the sandwich films. Figure 26 and Figure 27 have IR spectra from the same sandwich films as previously discussed. Because of the interference fringes mentioned above, we could not distinguish any chemical differences between likely good, likely bad, and likely bad with brake fluid using this technique.

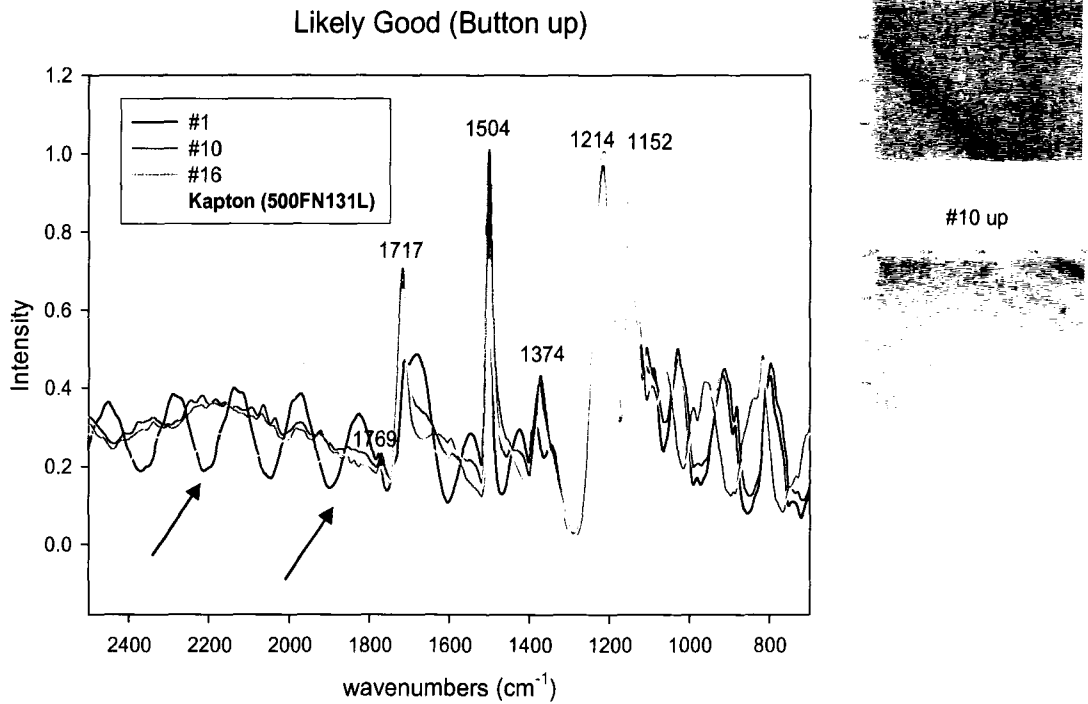


Figure 20: FT-IR reflectance spectra of “likely good” film sandwich and Kapton reference film and associated optical images

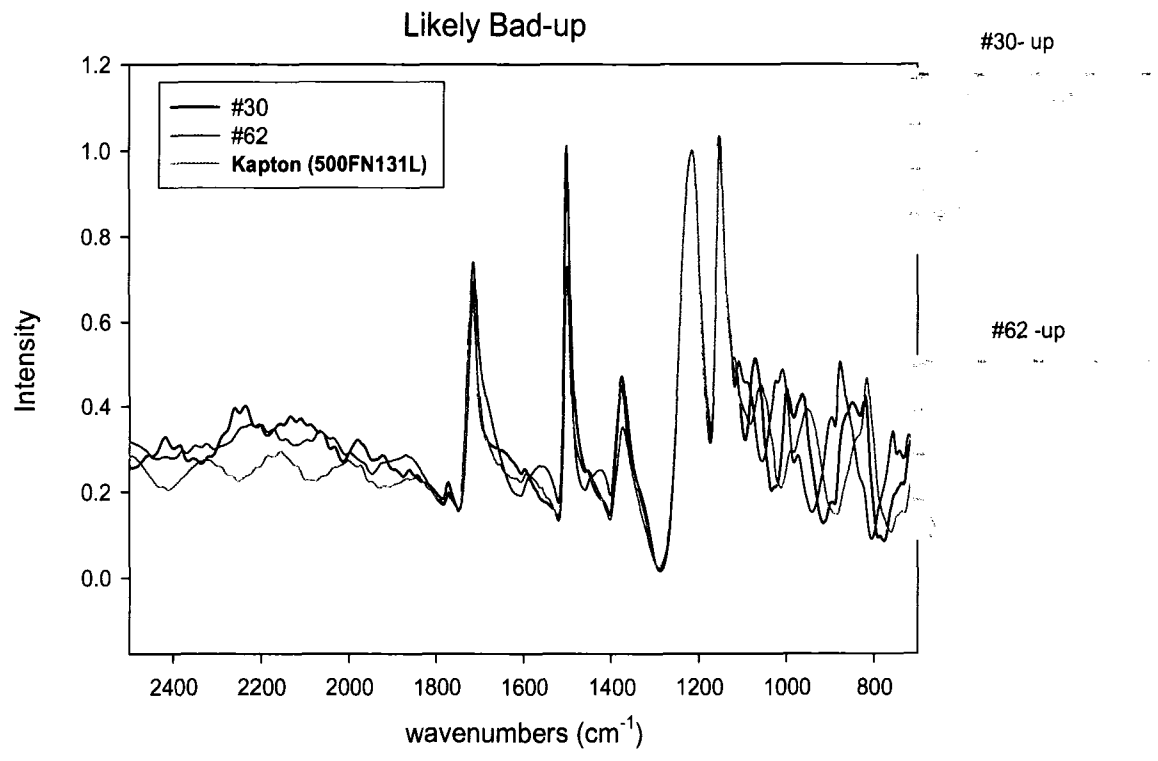


Figure 21: FT-IR reflectance spectra of likely bad film sandwiches and Kapton reference film and associated optical images.

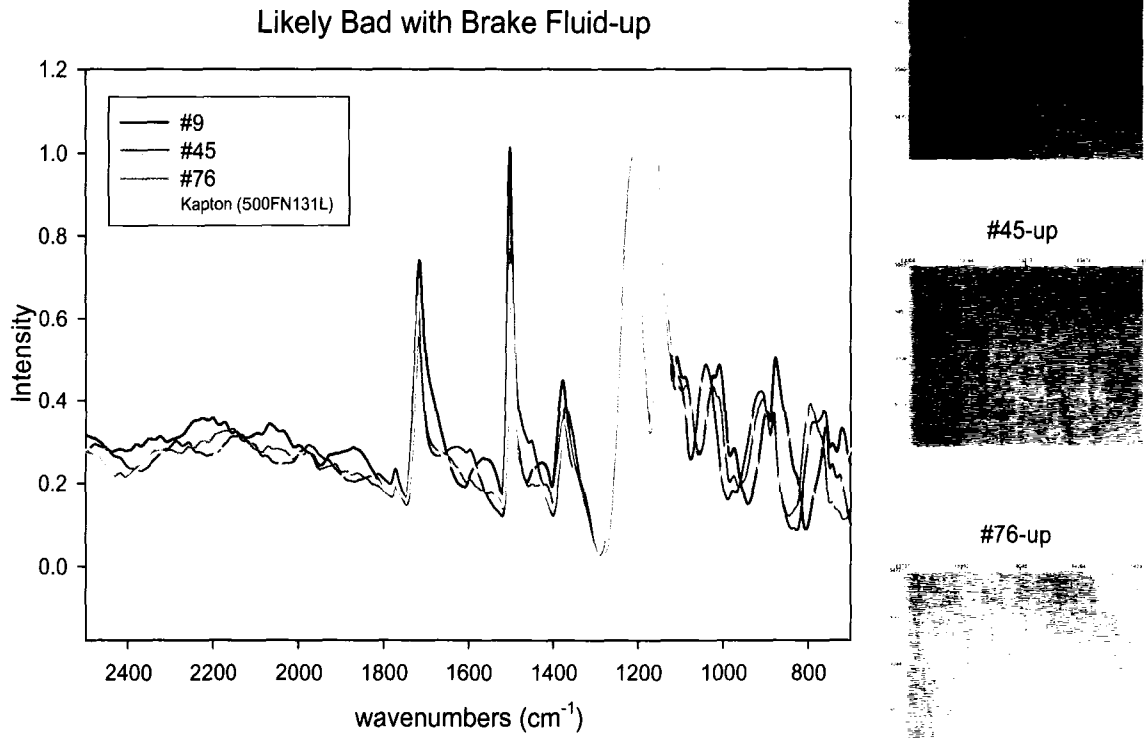


Figure 22: FT-IR reflectance spectra of likely bad with brake fluid film sandwich and Kapton reference film and associated optical images.

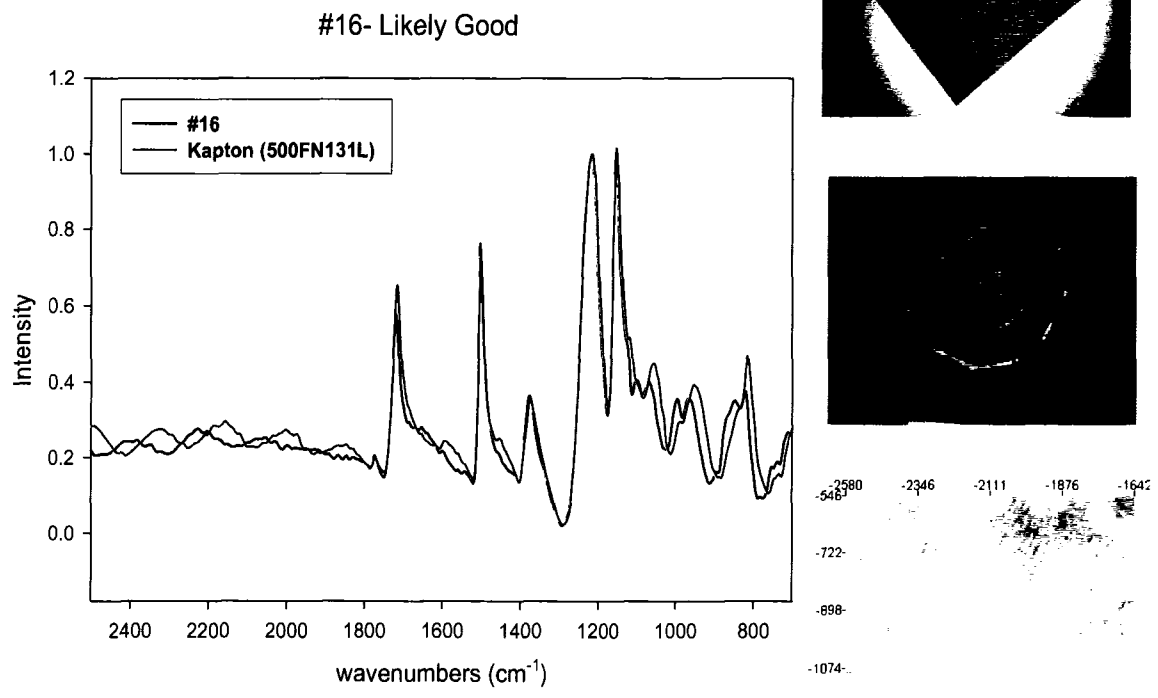


Figure 23: FT-IR reflectance spectra of likely good film sandwich and reference Kapton film and associated optical images.

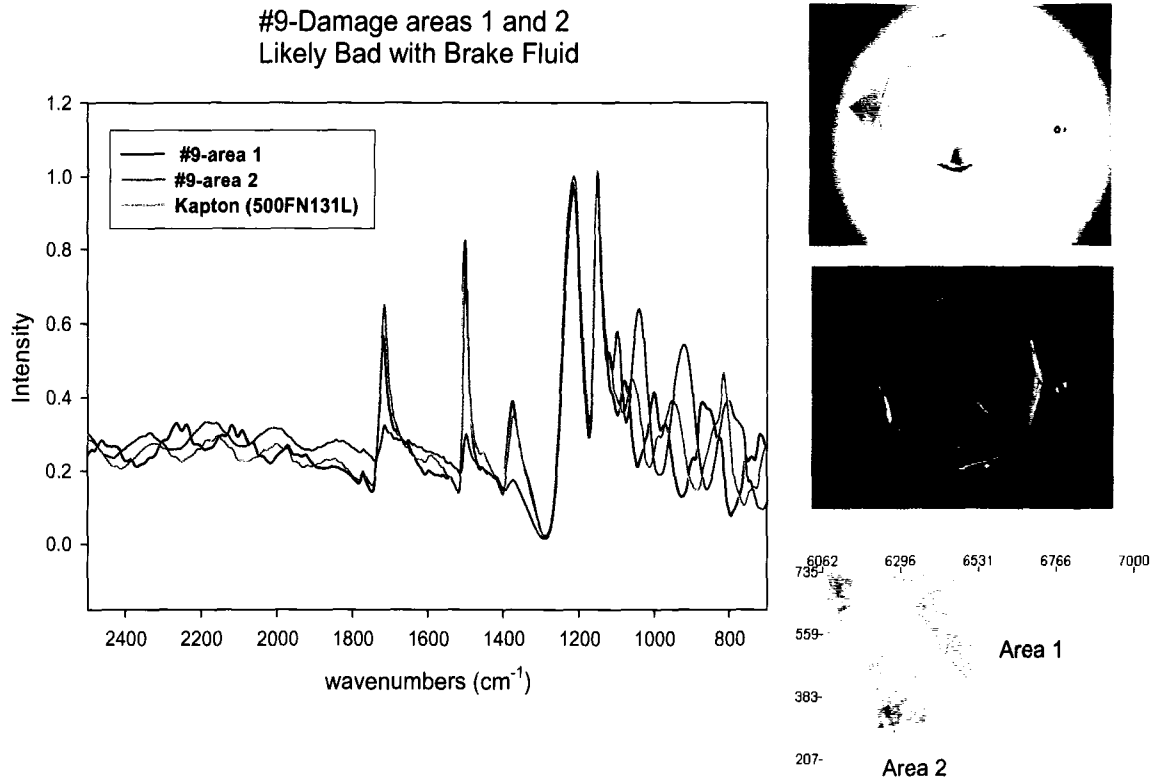
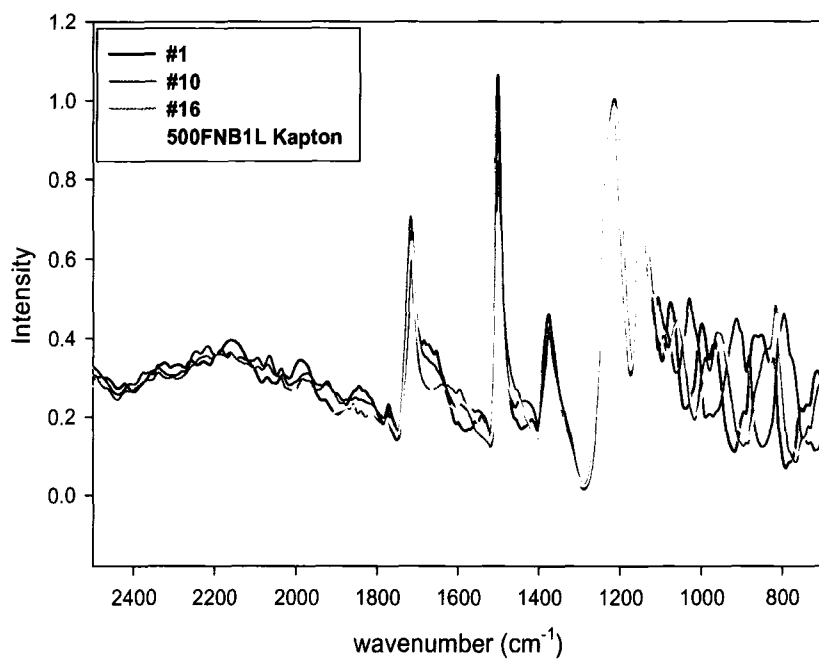


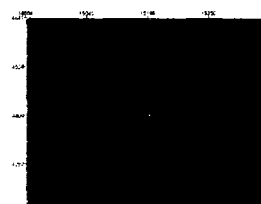
Figure 24: FT-IR reflectance spectra of damaged and undamaged areas and associated optical images.

"Button side" down

Likely good-down



#1-down



#10-down



Figure 25: FT-IR reflectance spectra of likely good sandwich films and associated optical images.

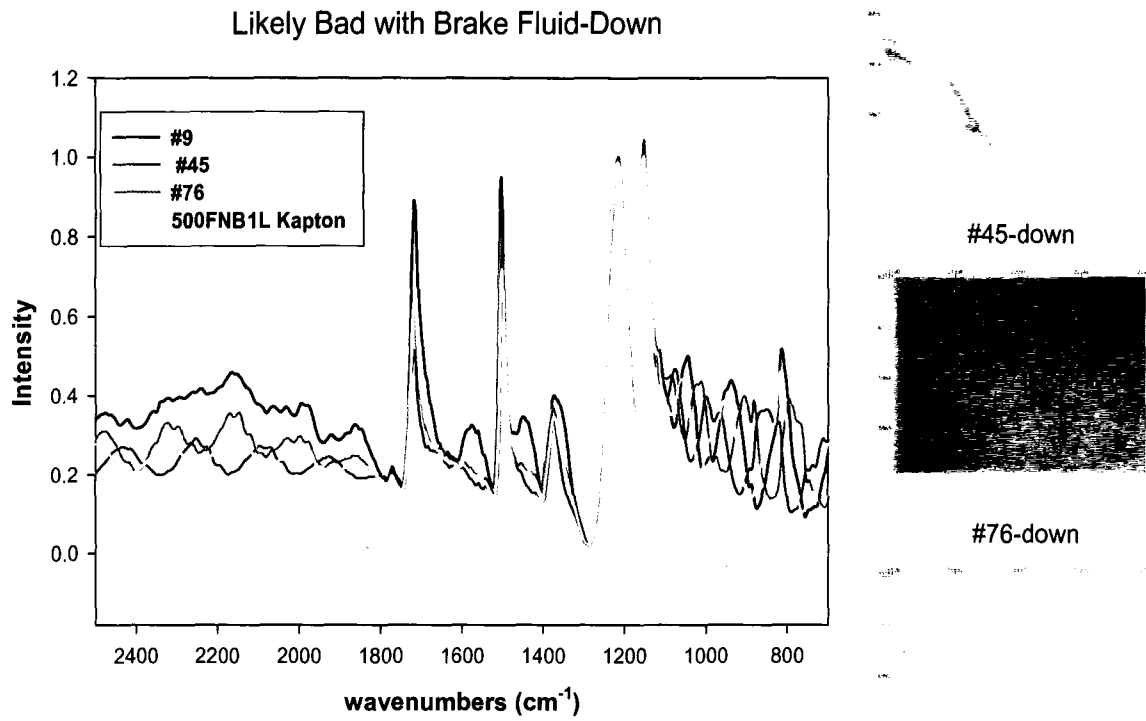


Figure 26: FT-IR reflectance spectra of likely bad with brake fluid sandwich films with associated optical images.

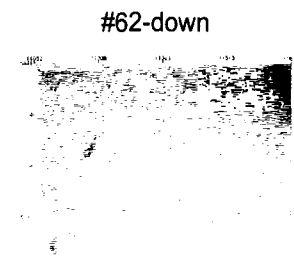
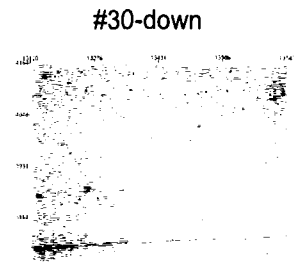
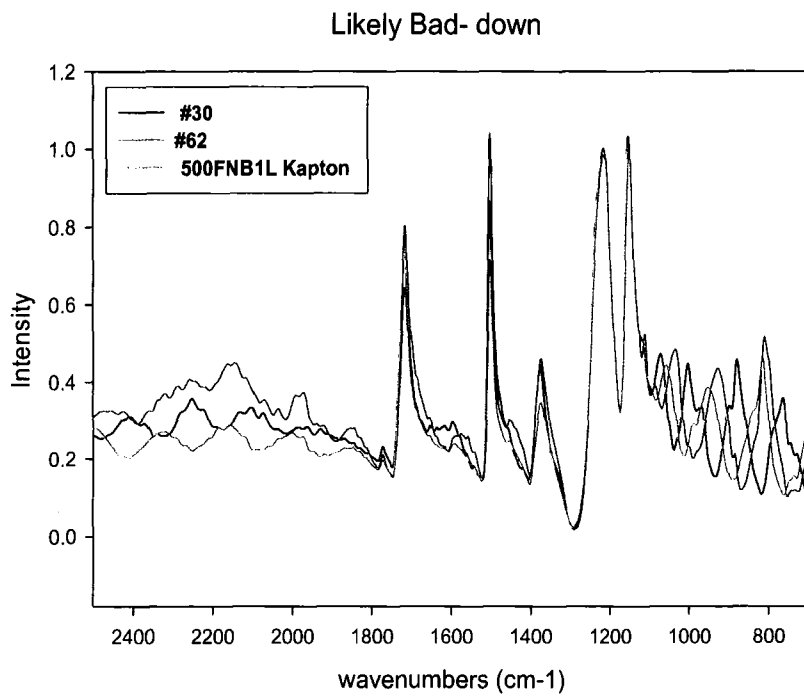


Figure 27: FT-IR reflectance spectra of likely bad sandwich films with associated images.

J. Thermal Analysis.

(1) *Thermogravimetric Analysis (TGA)*. A typical TGA scan is shown in Figure 28. Because the BWBR samples were clearly degraded, as can be seen in Figure 28, they have been excluded from the analysis of correlations between the other 4 categories. ANOVA analyses between the curves indicated only Transition 1 displays a statistically significant difference between the

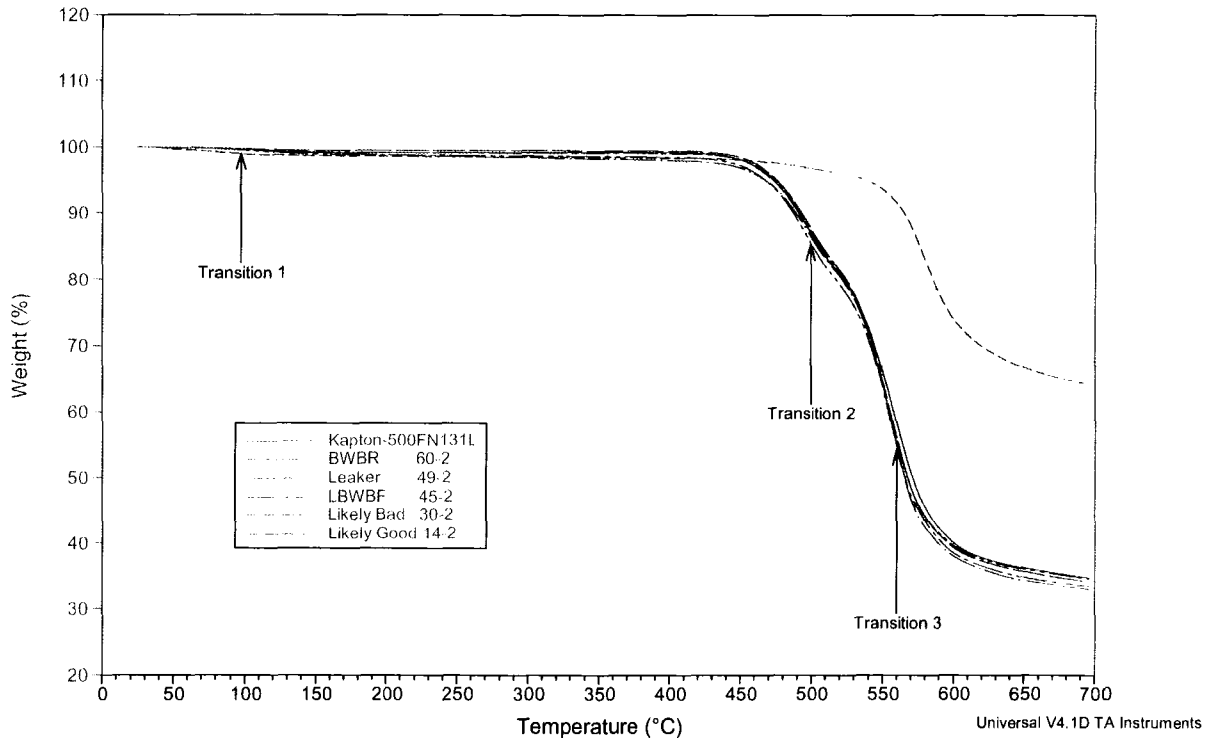


Figure 28. Sample TGA curves for all five categories of switches, plus an as-received Kapton-500FN laminate film.

four category of switches. Because of the temperature range and the known thermal stabilities of both Kapton and FEP, Transition 1 has been attributed to water loss. As can be seen in Table 20 below, the Leaker and LBWBF have a statistically significant higher content of moisture than

Table 20. Analysis of Mass Loss Attributable to Moisture Content

Category	# of Layers	Average Mass Loss (%)	Std. Dev. Of Mass Loss (%)
Likely Bad	18	0.51	0.02
Likely Good	54	0.63	0.02
LBWBF	14	0.97	0.02
Leaker	38	0.98	0.17

the Likely Good, whereas the Likely Bad has a lower moisture content. It is impossible to determine whether this slightly higher moisture content in the failed films is due to ingress of the moisture after failure of the FEP layer or whether it is related to FEP failure. The low moisture content of the Likely Bad switches might suggest the former; however, no definitive statement can be made at this point.

(2) *Differential Scanning Calorimetry*. Two primary endotherms (peaks in the DSC scan) were identified in all the classes of SCDSs. One peak is located around 115 °C and another around 250 °C. The lower peak is attributable to the glass transition of FEP and the upper endotherm the melting of crystals in the FEP layer. The glass transition had a large enthalpic relaxation component, i.e., instead of the step change in the heat flow typically observed with “clean” glass transitions, there was also a large enthalpic relaxation component, i.e., the peak on top of the step change. Because of the curvature in the baseline above and below the transition, the peak position of the enthalpic relaxation was examined rather than applying a typical glass transition analysis. No trend was detectable for the glass transition: 87 % of the 147 layers examined fell within the range of (124 ± 3) °C, and out of the remaining 13 % of the layers, 68 % were BWBR SCDSs. Because the glass transition overlaps the melting transition, no realistic estimates could be made regarding the heat of melting for the upper endotherm, however, analyses were performed on the peak positions. As can be seen in Figure 29 and Figure 30, there is a definite variation in the melting temperature, and as Figure 29 demonstrates, this even occurs within the Likely Good category.

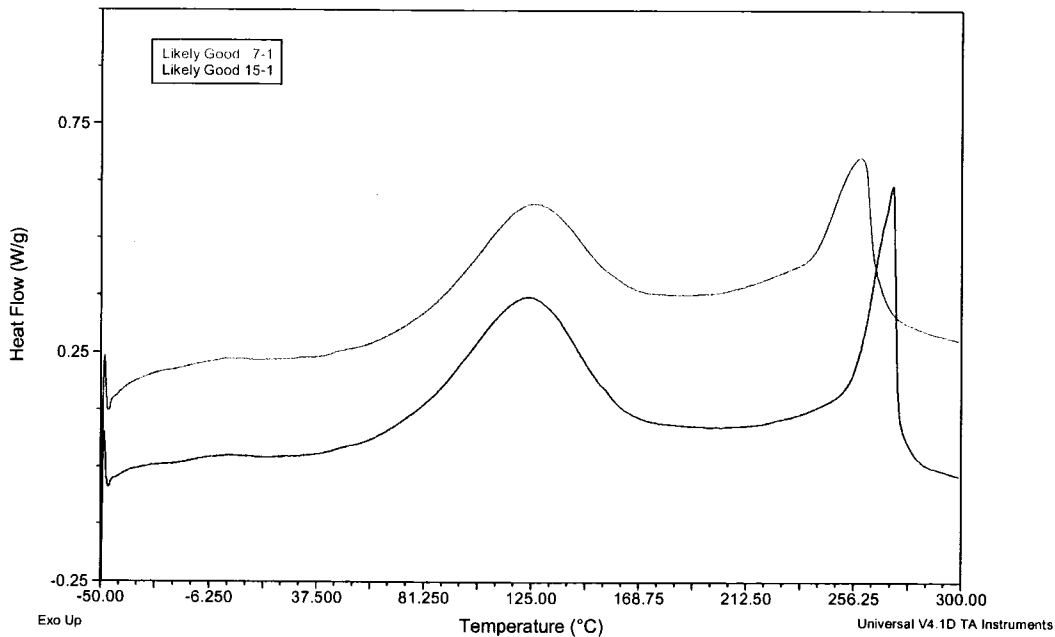


Figure 29. Typical DSC scans of two likely good switch components.

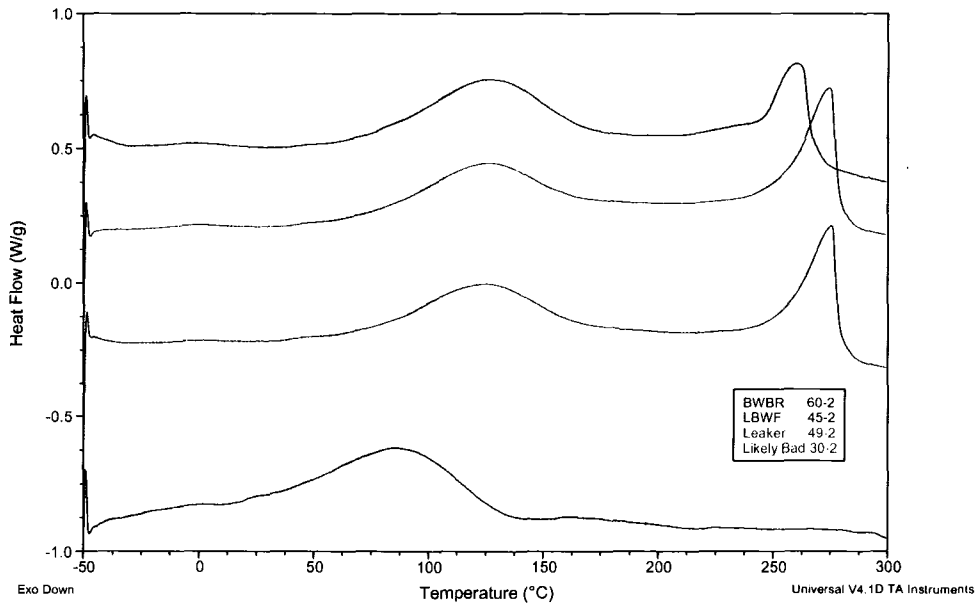


Figure 30. Typical DSC scans comparing “bad” and likely to go bad SCDS’s. (Note that these are the same SCDSs displayed in Figure 28.)

It is apparent from the LBWBR and BWBR DSC scans in Figure 30 that burning resulting in temperatures nearing or exceeding the melting point of the FEP crystals. In both case there is a change in the shape or loss of magnitude in the crystal melting peak.

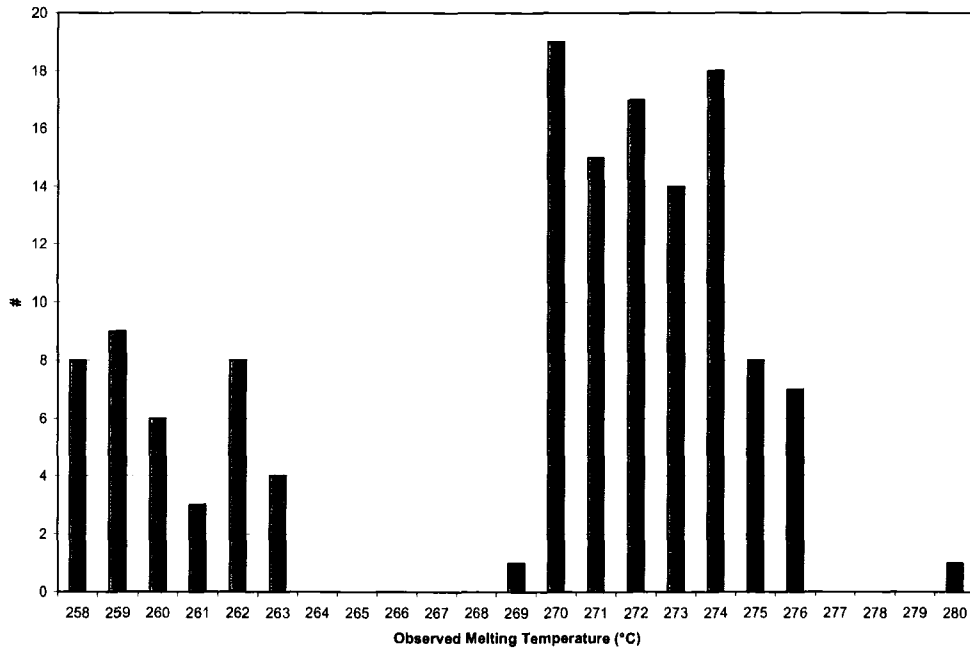


Figure 31. Number of layers with a given FEP melting temperature as a function of melting temperature.